2015

Development of Velocity Profile Generating Screens for Gas Turbine Components

Joseph Tate
University of Central Florida

DEVELOPMENT OF VELOCITY PROFILE GENERATING SCREENS FOR GAS TURBINE COMPONENTS

by

JOSEPH L. TATE
B.S. University of North Florida, 2009

A thesis submitted in partial fulfillment of the requirements
for the degree of Master of Science
in the Department of Mechanical, Materials and Aerospace Engineering
in the College of Engineering and Computer Science
at the University of Central Florida
Orlando, Florida

Fall Term
2015

ABSTRACT

Laboratory experiments on components of complex systems such as gas turbines require many conditions to be met. Requirements to be met in order to simulate real world conditions include inlet flow conditions such as velocity profile, Reynold's number, and temperature. The methodology to be introduced designs a velocity profile generating screen to match real world conditions through the use of perforated plates. The velocity profile generating screen is an array of jets arranged in a manner to produce sections of different solidities, a ratio of area that obstructs fluid flow compared to that of the total area. In an effort to better understand the interaction between perforated plate sections of different solidities, a collection of experimental data sets is presented to characterize the plates. This includes identification of fluid flow regions with characterization of the flow dynamics, though the analysis of velocity and turbulence decay. The aim of this characterization is to determine how the perforated plate's solidity affects the velocity development downstream and the location at which the velocity profile being produced can be considered complete.

TABLE OF CONTENTS

LIST OF FIGURES

LIST OF TABLES

LIST OF NOMENCLATURE

$M = Mesh\ Width$

$D = Diameter$

$CP = center\ of\ hole\ pattern$

$\dot{m} = mass\ flow\ rate$

$C_d = discharge\ coefficient$

$A_f = flow\ area\ (area\ created\ by\ holes)$

$A_d = downstream\ area\ (section\ area\ without\ holes)$

$\rho = density$

$e_{velocity} = velocity\ relative\ uncertainty$

$u_{dp} = dynamic\ pressure\ absolute\ uncertainty$

$u_T = ambient\ temperature\ absolute\ uncertainty$

$u_p = ambient\ pressure\ absolute\ uncertainty$

Y_o = mixing layer centerline offset

$\Delta P = pressure\ drop\ across\ the\ plate$

$Y = average\ expansion\ factor$

$\sigma = \frac{A_f}{A_d} = AR = area\ ratio\ (porosity)$

$1 - \sigma = solidity$

$v_d = downstream\ velocity$

$V = streamwise\ velocity$

$V_{JET} = jet\ exit\ velocity$

$dp = dynamic\ pressure$

$T_{atm} = ambient\ temperature$

$P_{atm} = ambient\ pressure$

$\delta = mixing\ \ layer\ width$

$\frac{d\delta}{dx} = spreading\ rate$

CHAPTER ONE: INTRODUCTION

In a power generation gas turbine, the velocity profile that exists at the interface of two components can often be quite complex because of multifaceted geometry and secondary flows. Difficulty arises when such velocity profiles need to be recreated in a laboratory in the absence of the upstream component. In an effort to better understand the importance of matching inlet conditions such as velocity profile a gas turbine's "MidFrame" will be used as an example. A power generation gas turbine's MidFrame, shown in Figure 1, is the component between the compressor and turbine which houses a set of diffusers and a combustor section.

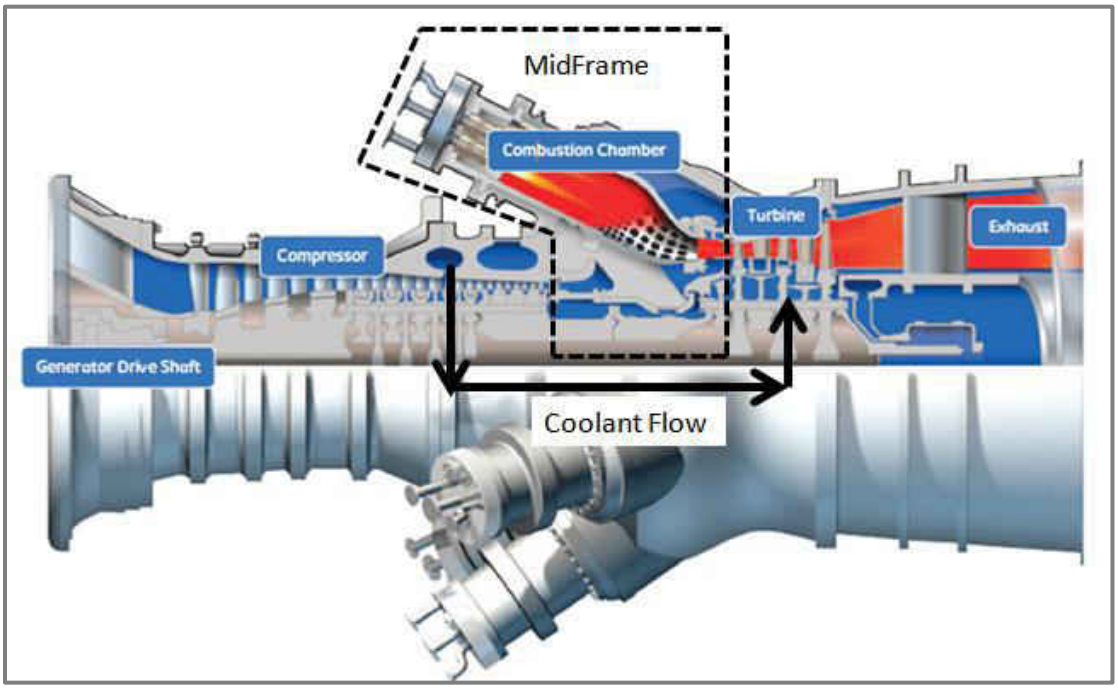

Figure 1: Power Generation Gas Turbine MidFrame

Figure 2 shows the flow field of a power generation gas turbine MidFrame. The MidFrame is designed to slow down the flow through a set of diffusers and then turn it towards the combustor in a manner to minimize losses. The flow then exits through the transition duct before entering the turbine where an example of a velocity profile is shown in Figure 2.

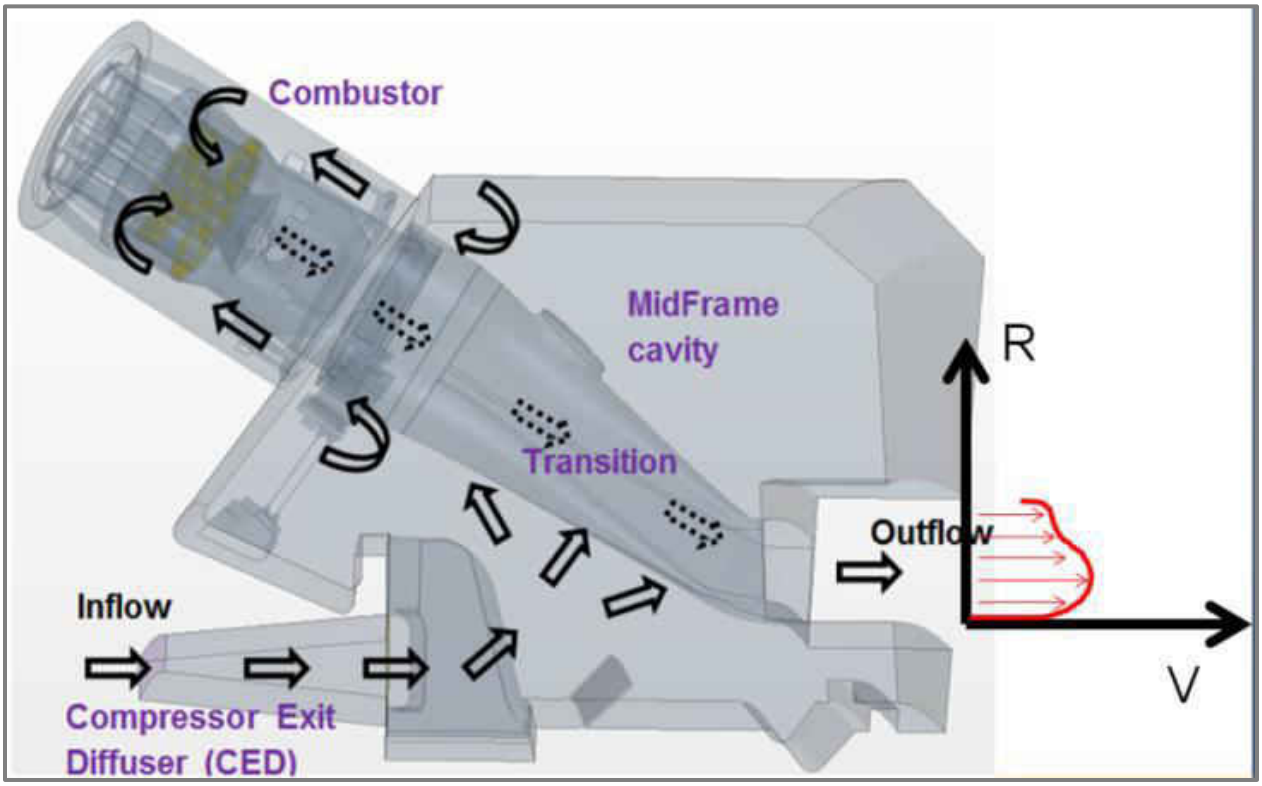

Figure 2: MidFrame Flow Direction

In an effort to better understand the flow field in the diffuser, dynamics in the MidFrame cavity, and decrease losses this component is tested with conditions as similar to real world conditions as possible. In Figure 3 an effort to visual the importance of the matching of the inlet velocity profiles is presented through the use of CFD. This CFD work was performed by Matt Golsen for his thesis (Golsen, 2011).

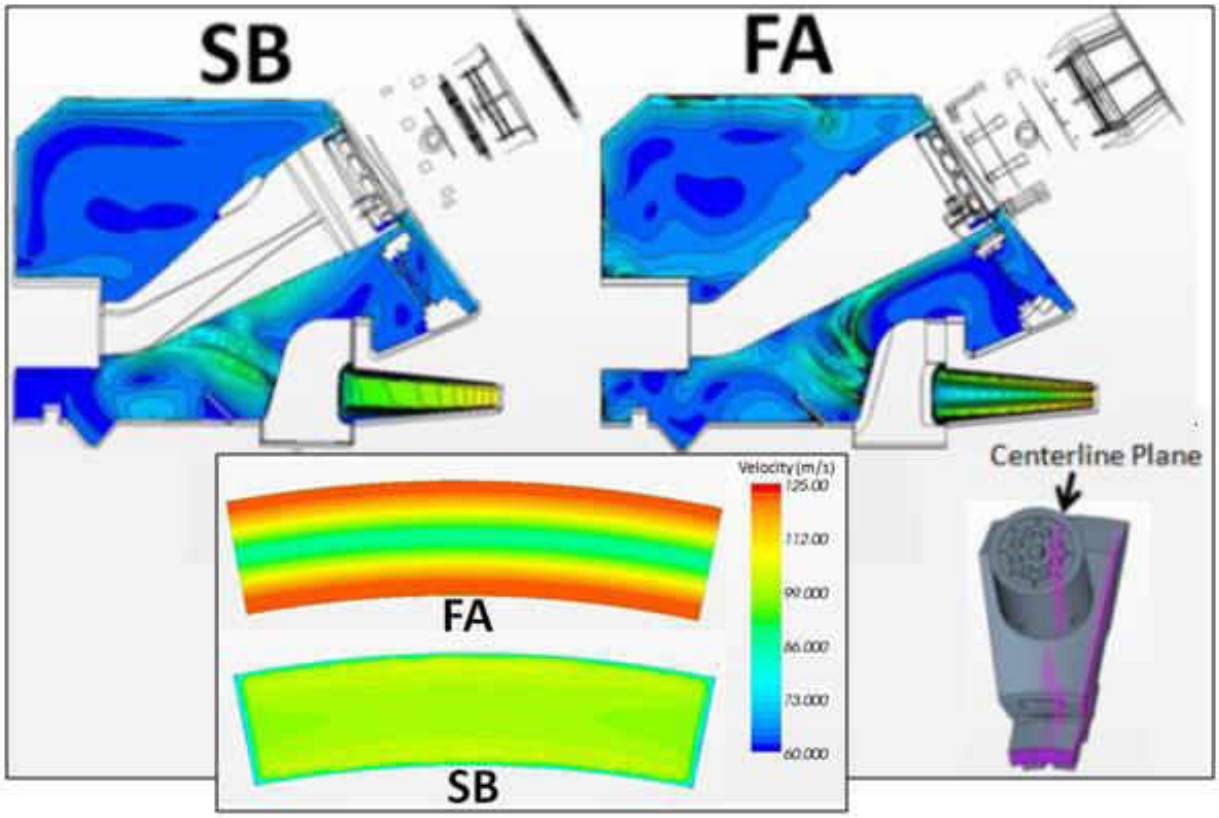

Figure 3: MidFrame CFD

In Figure 3, two different velocity profiles signified by the nomenclature FA, fully attached, and SB, separated bottom, are simulated as inlet conditions into the MidFrame using CFD. Difference in the flow activity of the MidFrame cavity section can be observed in the CFD. This difference in activity will result in differences in overall pressure loss and uniformity of the flow when entering the combustor section.

This paper will address the design philosophy, followed by validation, for producing a velocity profile generating screen using perforated plates to match a given radial velocity profile in an annular flow path with minimal pressure loss.

CHAPTER TWO: LITERATURE REVIEW

The screen being designed is intended to replicate velocity profiles in annular test sections for the testing of gas turbine components. To produce a symmetrical screen design inside of an annular section a perforated plate design is preferred over a wire mesh grid for its ease of manufacturing and flexibility in design. Velocity profile generation literature predominantly to this point has been focused on the use of wire meshes or gauzes. There are three pioneering works, found by the author, that have been the basis for a majority of the research on this subject matter. Owen and Zienkiewicz (Owen & Zienkiewicz, 1957) were one of the first to address the issue and their work was continued with research done by JL Livesey (Livesey, 1973) and others. The basic premise of this design methodology is to determine the screens resistance and deflection coefficients based on the screens geometry and assume that the upstream profile is uniform. The next methodology produced for velocity profile generation was produced by JW Elder (Elder, 1959). Elder's research was then furthered by researchers such as JT Turner (Turner, 1969). Elder expanded the velocity profile generation concept by increasing the number of screens that could be considered in the interaction with the flow and allowed for non-uniform upstream conditions. The third methodology, produced by McCarthy (McCarthy, 1964), is more limited on inlet conditions, but is applicable in three dimensions. The approaches presented primarily focused on the use of wire grids and will not be reviewed in depth. For an overview of the subject matter and the distinctions between the approaches refer to Laws (Laws, 1978).

One of the earlier works involving investigation of both perforated plates and wire mesh screens was performed by Baines and Peterson (Baines, 1951). Baines and Peterson investigated the dependence of velocity and turbulence downstream of a screen to that of the upstream conditions. The problem encountered in this investigation was that instabilities were observed downstream of screens with high solidity. Solidity refers to the amount of solid area occupied by the screen compared to that of the total area. In general the higher the solidity the more resistance the screen has in the flow. The opposite of solidity is porosity, a ratio comparing the amount of flow area not occupied by the screen compared to the total area. A similar group of screens was investigated by Roach (Roach, 1987). In this work, an updated assessment incorporating more current decay functions was provided. Roach however, had a similar problem as Baines in that there were only high solidity perforated plates tested which saw similar flow instabilities. Researchers such as Castro and Villermaux investigated this high solidity phenomenon and found that for perforated plates of solidity higher than approximately 0.5, there was an oscillatory instability associated with the merging distance of the jets.

Other investigations involving perforated plates and screens of lower solidity at various inlet conditions include the various works completed by Tan-Atichat, Loehrke and Nagib (Tan-Atichat, 1982). Loehrke provides one of the few complete data sets available in this regard. Rui Liu is another researcher who completed multiple tests of perforated plates including an investigation on the influence of perforated plate geometry on isotropic turbulence (Liu, 2004). The research done by Liu includes multiple solidities and inlet conditions.

Fluid interactions with perforated plates and wire meshes have been studied for quite some time. The predominate area of research involving the fluid interactions with screens is the study of isotropic turbulence produced downstream of the screen. This area of research provides a good base for learning the fundamentals of turbulent flow. The most complete data set found for screen generated isotropic turbulence, is that assembled by Mohamed and Larue (Mohamed & Larue, 1990). The investigation completed provides a methodology for identifying the region where turbulence can begin to be considered locally isotropic. Mohamed and Larue consolidated data from a majority of the well-established works on the subject of grid turbulence and devised criteria for comparison. This region of locally isotropic turbulence is predominately reached downstream of a screen or perforated plate in regions referred to herein as the Mixing and Developed Region. The flow field regions are depicted in Figure 4 using the interaction between two individual jets is used as an example.

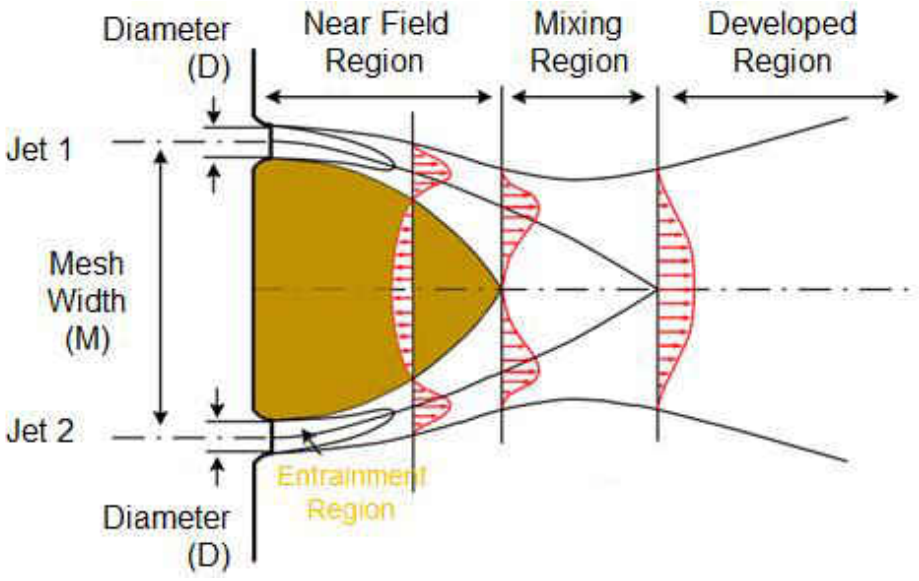

Figure 4: Flow Field Regions

The Near Field region is where the jets produced by the screen or perforated plate behave in a manner similar to that of axisymmetric free jets. This is also the region where turbulent kinetic energy is produced and reaches a maximum. Downstream of the Near Field Region in the Mixing Region where the jets start to interact with each other. This is also the region where turbulent intensity begins to decay. The ultimate goal of the velocity profile generating screen is to produce a smooth velocity profile which can be considered completed in the Developed Region. The regions of interest for this investigation are the regions after the Near Field Region. One of the few studies focused on fluid interaction with perforated plates in the Near Field region is that undertaken by Stefan Horender (Horender, 2013). Horender focuses on high solidity plates, but does provide a base for comparison. The last case study to be introduced on the subject matter of perforated plates is that which was completed by Svensson (Svensson, 2015). The geometry of the perforated plates tested is not the same as those presented here, but they do present a similar trend and a complete analysis including analysis of the fluid flow regions downstream of the Near Field Region.

The final design component of the velocity profile generating screen is the interaction of jets from sections of different perforated plate solidities. This general concept is comparable to that of plane mixing layers. This area of research is well documented and is detailed on many different aspects. The most common experimental procedure for studying plane mixing layers includes the use of a splitter plate. This splitter plate aims to provide interaction between two streams of different uniform velocities. R.D. Mehta provides a comprehensive data set including a range of velocity ratios, but the initial condition includes a developed boundary layer on the

splitter plate (Mehta, 1991). Other investigations on the subject matter more applicable to this set up include works such as that performed by Tavoularis (Tavoularis, 1987). In this set up Tavoularis makes an effort to provide a turbulent initial condition to show proof that the resultant velocity profile is independent of the initial condition. Tavoularis uses an arrangement of screens, channels, and rods to develop a desired velocity ratio and turbulence level. This data supports the idea that even with high initial turbulent conditions that plane mixing layers are self-preserving free turbulent flows.

CHAPTER THREE: METHODOLOGY

The characteristics to describe the fluid dynamics in the flow through perforated plates used in this design were obtained from research performed by Matthew Van Winkle (Winkle & Kolodizie, 1957). The research completed by Winkle provides a connection between flow resistances based on Reynolds number to the perforated plate's geometry. The perforated plates tested by Winkle included a variety of hole diameters and thicknesses. The perforated plate design used for this investigation is machined in-house from ¼" acrylic. Before introducing the design elements of Winkle's research an overview of the screen geometry is required to introduce nomenclature. The perforated plate pattern being used in this design is of a staggered variety that allows for a consistent pattern around an annular section. The holes of the pattern have a diameter, D, and are located at the ends of an equilateral triangle with sides equal to the mesh width, M, shown in Figure 5.

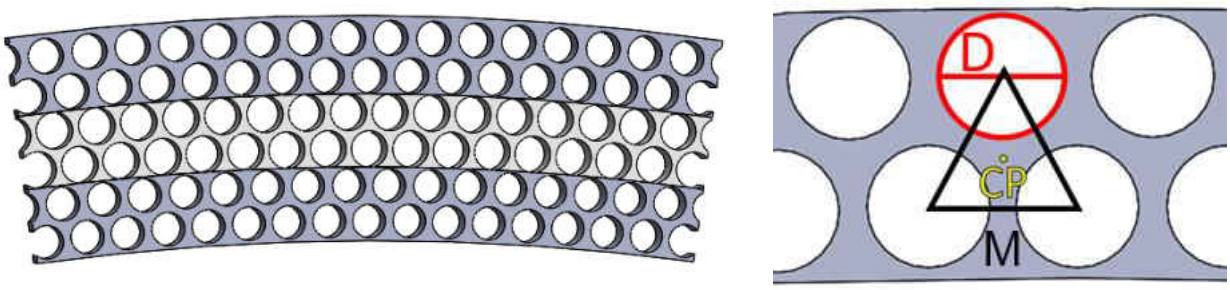

Figure 5 : Perforated Plate Geometry

The annular screen is divided into multiple sections and is shown as a three section design differentiated by a variation in color in Figure 5. Each section has its own specified mesh width, M, to allow for consistent spacing. The mesh width of each section increases from bottom to top to allow the pattern to be consistent circumferentially. Varying the hole diameter of the different annular sections in the screen, changes the solidity/porosity, allowing for different velocities at different radial positions.

With the hole locations set for the screen design, the desired velocity profile is achieved by varying the diameter of the holes, thus the flow area. The calculation for the hole diameters is based off of the work done by Winkle (Winkle & Kolodizie, 1957). The discharge coefficient is the main characteristic investigated by Winkle to describe the relationship of the perforated plate geometry to flow resistance. The discharge coefficient relation is shown in a general form below in Equation (1).

$$\dot{m} = C_d * A_f * Y * \sqrt{\frac{2 * \rho * \Delta P}{1 - \left(\frac{A_f}{A_d}\right)^2}} \quad \textbf{(1)}$$

General Discharge Coefficient

This equation accounts for the viscous losses produced by the introduction of a perforated plate into a flow. The losses are accounted for by relating mass flow obtained in testing of a given geometry to that of the theoretical mass flow. Equation (1) is the most common equation seen in the evaluation of perforated plates, wire mesh screens, orifice plates, Venturi nozzles, and other similar devices. Equation (1) includes a parameter, the expansion coefficient (Y), which can be

neglected in our evaluation of the velocity profile generating screen. The expansion coefficient accounts for the density change as a fluid passes through a contraction due to the static pressure drop. This factor is best visualized using the relation produced by Stearns in Figure 6 (Stearns, 1951). This figure gives a relationship between area ratio, static pressure drop, upstream absolute static pressure, and expansion coefficient. In the case of the MidFrame suction rig this screen is to be tested in, the absolute static pressure is on the order of 100000 Pa and the pressure drop is on the order of 5000 Pa. This gives a pressure ratio, $\Delta P/P_1$, on the order of 0.05 and corresponds to a negligible expansion coefficient. The velocities obtained in the acceleration of the fluid through the perforated plate are also of a sufficiently low Mach number that this will be treated as an incompressible case.

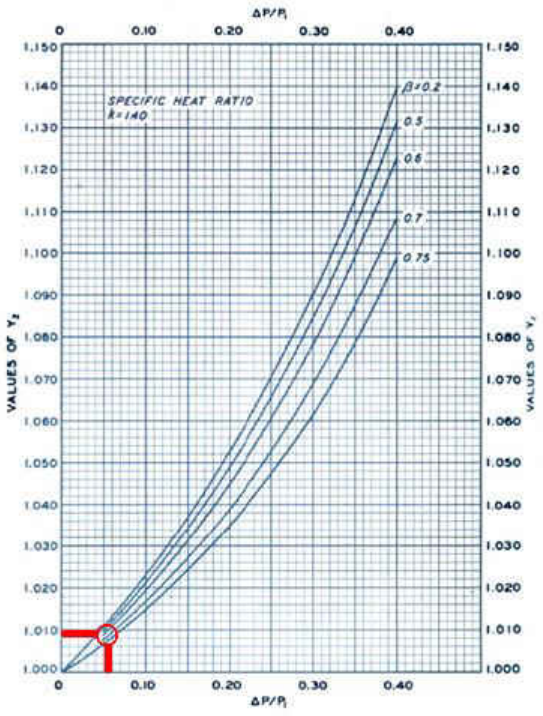

Figure 6: Expansion Coefficient

Equation (1) can be transformed into Equation (2) to better show the relationship of the perforated plate geometry to its effect of the flow.

$$C_d{}^2 * \frac{\sigma^2}{1-\sigma^2} = \frac{\rho * v_d{}^2}{2 * \Delta P} \quad \textbf{(2)}$$

Pressure Resistance

The left side of this equation is a ratio based on the perforated plate's porosity, σ, multiplied by the discharge coefficient. The right side of the equation gives a ratio of static pressure drop to the dynamic pressure. If the flow, dynamic pressure, is held constant along with the discharge coefficient an increase in porosity relates to a lower pressure drop. Another way to look at this equation is if the static pressure drop and discharge coefficient are held constant an increase in porosity equates to a higher velocity. Equation (2) can be used with supplied inlet velocity profile data at specific radial positions to determine each screen section's hole diameters. The specific radial locations used from the provided velocity profile data coincides with the center of the hole pattern (CP) of each screen section, refer to Figure 5. The downstream velocity (v_d), specified by the provided velocity profile, is proportional to the area ratio (porosity) shown in Equation (3). The porosity is a ratio of the flow area compared to the total downstream area. The downstream area, shown in Equation (4), is determined using the mesh width, M, of the given section. The flow area, shown in Equation (5), is based on the area occupied by the holes inside the equilateral triangle used to locate them, refer to Figure 5.

$$\sigma = \frac{A_f}{A_d} \tag{3}$$

Area Ratio (Porosity)

$$A_d = \frac{\sqrt{3}}{4} * M^2 \tag{4}$$

Downstream Area

$$A_f = \frac{1}{2} * \pi \left(\frac{D}{2}\right)^2 \tag{5}$$

Flow Area

The problem that arises with Equation (2) is that the discharge coefficient is not only dependent on the area ratio, but also the diameter of the holes and the thickness of the material used to produce the screen. For this application an equation was derived for the discharge coefficient from the data provided by Winkle's research (Winkle & Kolodizie, 1957). This equation is for a given material thickness, in our case ¼", and an application where the Reynolds number is sufficiently large enough that the discharge coefficient is constant. The general trend and curve fit is shown in Figure 7 with the full equation below in

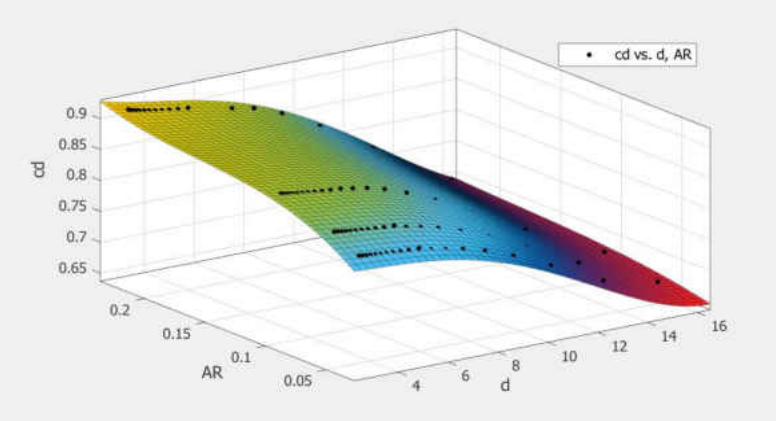

$C_d = discharge\ coefficeint$

$AR = Area\ Ratio\ (porosity)$

$d = hole\ diameter$

Figure 7: Discharge Coefficient Curve Fit

$$C_d = 0.7693 - (0.006757 * d) + (2.506 * AR) + (0.002876 * d^2) - (0.1678 * AR * d) - (14.4 * AR^2) - (0.000413 * d^3) + (0.01011 * AR * d^2) + (0.704 * d * AR^2) + (31.21 * AR^3) + (0.0000141 * d^4) - (0.0004095 * AR * d^3) - (0.0007536 * d^2 AR^2) - (1.564 * d * AR^3) \quad (6)$$

Discharge Coefficient

This equation provides more information upon examination. One of the main criteria for the design of this screen is to manipulate the velocity profile with minimal pressure drop. For a majority of the geometric designs chosen that meet this criteria, those of high porosity, the discharge coefficient obtained from the derived equation are larger than unity. When this occurs the discharge coefficient is designated to be the real world maximum of 1.

To solve this equation an initial assumption for the hole diameter where the maximum velocity is located is required. This diameter is determined to provide the lowest possible pressure drop, but still provide a structurally sound screen that would withstand the testing environment. To

accomplish this, a porosity of 0.7 was chosen for the screen section with the highest velocity. This porosity was the largest that with the current material and manufacturing techniques could consistently be achieved without the screen breaking in testing. The setting of this value allows for the discharge coefficient and static pressure drop across the screen to be determined. The static pressure drop is assumed to be constant across all the sections. This assumption is demeaned valid with the application of boundary layer theory used in the investigations of jets and most free shear flows investigated hear in. Knowing the pressure drop across the screen, a given velocity profile can be used to determine the diameter of the holes for the remaining sections.

With the methodology presented, the resulting velocity profile match left room for improvement. In an effort to improve the understanding of flow through a perforated plate, the design elements for the velocity profile generating screen were examined to determine those that would provide the most useful test data in a specialized rig. The geometric elements that were fixed were the overall size, hole pattern mesh width, and inlet conditions. The screen was changed to a 6 inch square to fit in a test section that was purpose built for this application. The hole pattern mesh width was set to allow the variation of the hole diameter to determine the porosity of the screen. To provide a comparable data set, a consistent mass flow was used to produce a constant upstream velocity and turbulent intensity between the screen tests.

CHAPTER FOUR: EXPERIMENTAL SET UP

Experiment 1

In an effort to improve the accuracy of the velocity profile generating screen design three different experiments were conducted. Experiment 1 was conducted to show proof of concept and evaluate the previously mentioned design methodology. In this experiment a screen was produced based on a provided velocity profile and tested in an annular section, show in Figure 8.

Figure 8: Annular Test Section with Screen

In this experiment it was desired to identify what parameters were contributing to the error associated with the production of a desired velocity profile. This annular test section is attached to a MidFrame test section run under suction. Upstream of the annular test section is a double contraction plenum with multiple screens and honeycomb sections to help suppress any

disturbances. Downstream of the screen, plastic inserts were installed on the walls to provide the smoothest surface possible to allow for the most accurate measurement possible. The annular test section has a slot in the bottom wall 279.4 mm (11 inches) downstream of the screen to allow for a 1.59 mm (1/16”) pitot static probe to be inserted in the flow and traversed. A picture of the traversing system which includes both radial and circumferential components is shown in Figure 9.

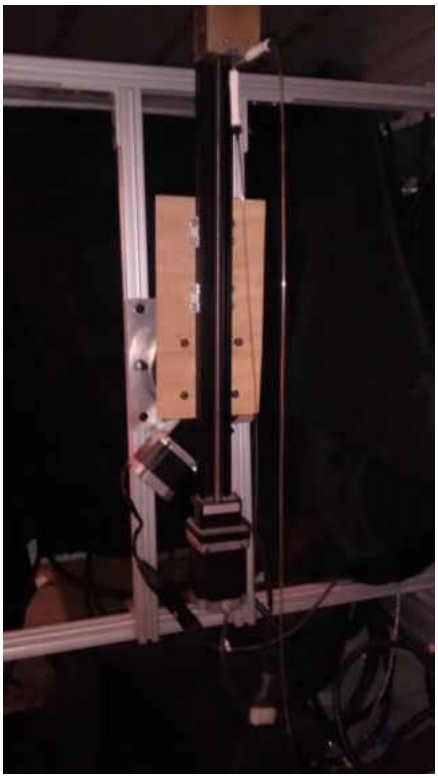

Figure 9: Annular Test Section Traverse System

Due to the pitot static probes sensitivity close to a solid boundary, measurements up to 5 diameters of the probe will be neglected in this experiment. In the annular test section a grid of 20 radial points and 5 in the circumferential direction will be taken to give an evaluation of the screen generated velocity profile and its uniformity. The experiment was conducted using a

pressure transducer system from Scanivalve to take the gauge pressure measurements. The Scanivalve system used a 5 psi transducer which took 30 measurements of both total and static gauge pressure for each position. These measurements were taken 4 seconds after the traverse arrived at each position to allow for the pressure to equalize in the lines. The 30 samples were taken with a delay of 0.25 seconds between samples. A generic desktop barometer and a Fluke 52II thermocouple reader were used to collect the ambient conditions. This test equipment combined to offer a velocity measurement relative uncertainty, for the ranges tested, of approximately 2%. This relative uncertainty was obtained through an uncertainty propagation analysis shown below in Equation (7).

$$e_{velocity} = \sqrt{\frac{1}{4}\left(\frac{u_{dp}}{dp}\right)^2 + \frac{1}{4}\left(\frac{u_T}{T_{atm}}\right)^2 + \frac{1}{4}\left(\frac{u_P}{P_{atm}}\right)^2} \quad (7)$$

Velocity Relative Uncertainty

Experiment 2

This proposed experiment consisted of testing four single solidity screens with various porosities measuring axial velocity distributions at various positions downstream of the screen. This experiment aimed to produce a baseline for velocity decay downstream of specific single solidity perforated plate. The axial velocity was measured by using a constant temperature anemometer mounted to a three dimensional traversing system. After conducting a few sample data sets to conduct a convergence study it was determined that the data was to be collected at a sampling rate of 25000 Hz for a sampling period of 5 seconds. This was done using a TSI IFA 300 with

the hot wire calibrated using a TSI Automated Air Velocity Calibrator Model 1129. The relative uncertainty associated with these measurements is approximately 3%. This uncertainty was obtained in an uncertainty propagation analysis and can be seen in detail in guide produced by Dantec Dynamics (Jorgensen, 2002).

The test rig consisted of wind tunnel attached to the pressure side of a centrifugal blower. The test section is preceded by a settling chamber and contraction section. The settling chamber consisted of multiple honeycombs and mesh screens to reduce turbulence and non-uniformities. The test section has been tested without a perforated plate to verify inlet turbulent intensity at the inlet. The mass flow was held constant between each test and resulted in an average velocity of approximately 33 m/s. The turbulent intensity was shown to be on the order of 0.5%-1% for this testing condition. Shown in Figure 10 is a picture of the test section including one of the perforated plates tested. Figure 10 also includes coordinate orientation and an indication of where the hotwire was inserted into the bottom of the wind tunnel.

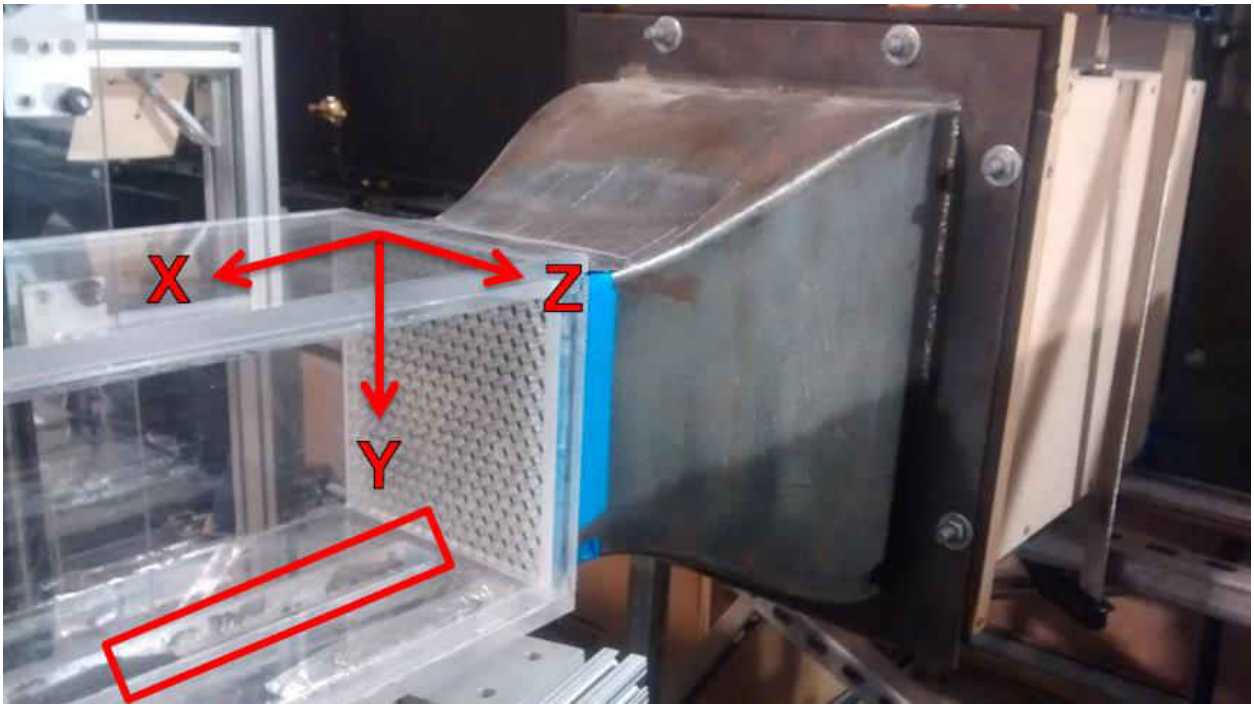

Figure 10: Test section picture

Figure 11 shows a CAD of the test section with test data to visualize the locations downstream of the screen measured. The axial locations, measured from the backside of the screen, are listed in the figure as well.

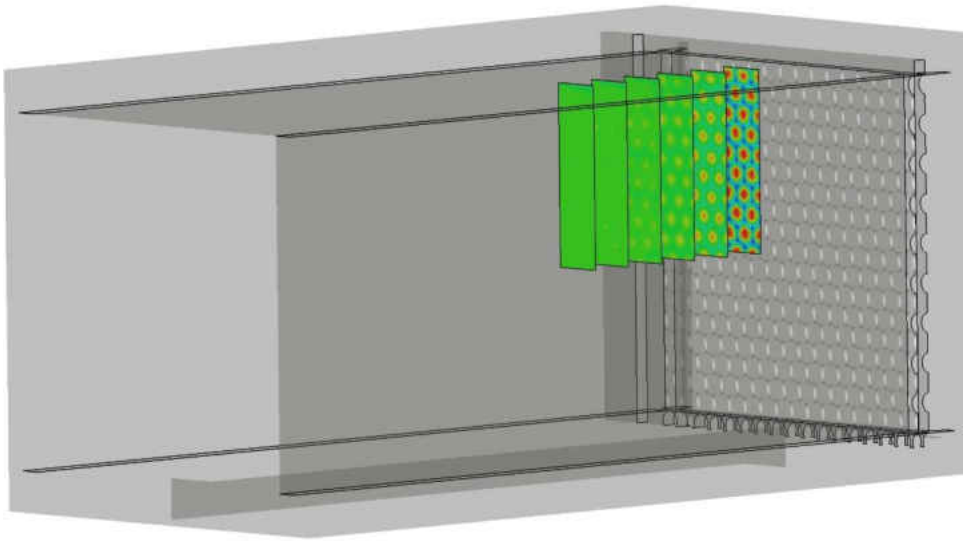

Downstream Locations (X)
12.7mm (0.5”)
31.75 mm (1.25”)
50.8 mm (2”)
69.85 mm (2.75”)
88.9 mm (3.5”)
109.75 mm (4.25”)
127 mm (5”)
146.05 mm (5.75”)
165.1 mm (6.5”)
184.15 mm (7.25”)
203.2 mm (8”)
222.25 mm (8.75”)

Figure 11: Test Section CAD with test locations for Single Solidity Test

The grid traversed is listed in Table 1. The axis orientation used for testing is shown in Figure 10. The flow direction is X with the origin located at the backside of the screen. The vertical direction is Y with the origin set at the test section top wall. Vertically down is set to be the positive Y direction. The horizontal direction parallel to the screen is Z with the origin at the beginning plane of the traverse (approx. 0.5” off centerline).

Table 1: Single Solidity Traverse Grid

	Number of Intervals	Interval Separation
X	6	19.05 mm (0.75”)
Y	66	1.22 mm (0.0479”)
Z	10	2.44 mm (0.096”)

The range of screen porosities tested was determined by those used in the velocity profile generating screen. The porosities chosen provided a low pressure drop, were structurally sound, and have a discharge coefficient equal to unity. Listed in Table 2 are the dimensions of the screens tested.

Table 2: Single Solidity Screen Dimensions

	Hole Diameter	Screen Porosity
Screen 1	7.938 mm (5/16”)	0.5978
Screen 2	8.334 mm (21/64”)	0.6591
Screen 3	8.5 mm (0.335”)	0.6855
Screen 4	8.731 mm (11/32”)	0.7234
All Screens have a mesh width of 9.779 mm (0.385”)		

Experiment 3

Experiment 3 uses the same wind tunnel and measuring device as Experiment 2, but with different screens and measuring increments. Experiment 2 provided a baseline of how jets

interact in a single solidity screen or a uniform free stream. Experiment 3 expands upon this experiment by adding a second solidity to the screen to investigate the interaction between jets of different solidity screens. The screens to be tested are listed in Table 3. In Table 3 is some information pertaining to the difference between solidity and velocity ratio. These two terms are inversely proportional. As the difference in porosity between the two sections decrease the velocity ratio increase showing the velocities are closer together. Figure 12 shows a CAD of the test section with test data to visualize the locations downstream of the screen measured. The axial locations, measured from the backside of the screen, are listed as well in the figure.

Table 3: Mixed Solidity Screen Dimensions

	Porosity 1	**Porosity 2**	**Porosity Difference**	**Velocity Ratio**
Screen 5	0.69	0.66	0.03	0.96
Screen 6	0.72	0.66	0.06	0.92
Screen 7	0.69	0.6	0.09	0.87
Screen 8	0.72	0.6	0.12	0.83
All Screens have a mesh width of 9.779 mm (0.385”)				

The other deviation from the Experiment 2, besides the screens tested, is an adjustment to the grid being traversed. The X and the Z direction are expanding to supply a larger data set shown below in Table 4.

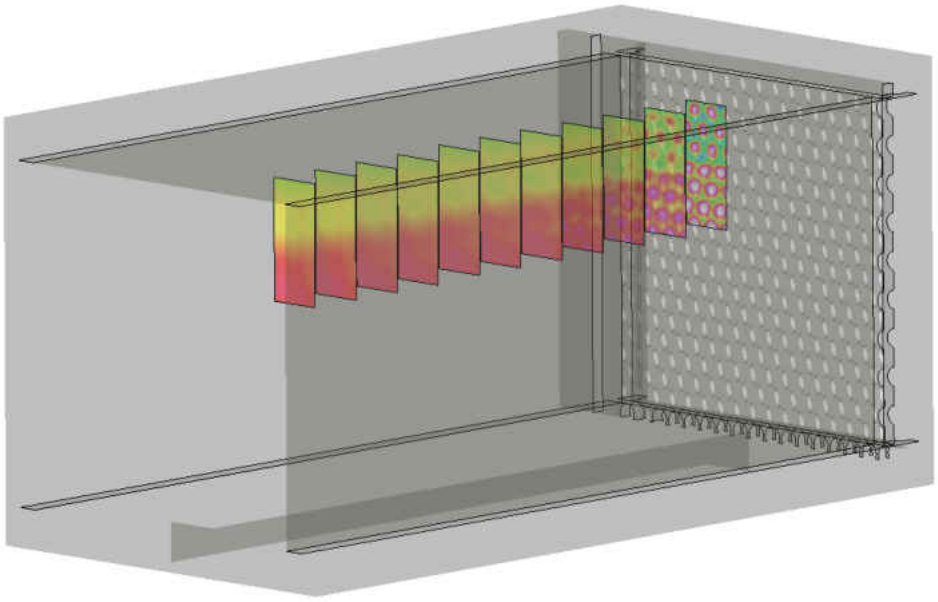

Downstream Locations (X)
12.7mm (0.5”)
31.75 mm (1.5”)
50.8 mm (2.5”)
69.85 mm (3.5”)
88.9 mm (4.5”)
109.75 mm (5.5”)
127 mm (6.5”)
146.05 mm (7.5”)
165.1 mm (8.5”)
184.15 mm (9.5”)
203.2 mm (10.5”)

Figure 12: Test Section CAD with test locations for Mixed Solidity Test

Table 4: Mixed Solidity Traverse Grid

	Number of Intervals	Interval Separation
X	11	25.4 mm (1”)
Y	66	1.22 mm (0.0479”)
Z	11	2.44 mm (0.096”)

CHAPTER FOUR: FINDINGS

Experiment 1

For the proposed experiment a selection of velocity profiles need to be designated for evaluation. In an effort to simulate velocity profiles similar to those commonly encountered in a power generation gas turbine MidFrame, a selection of velocity profiles found in compressors were chosen. Leroy Smith provided the velocity profiles to be evaluated in his paper *Casing Boundary Layers in Multistage Axial-Flow Compressors* (Smith, 1970). One of the velocity profiles comes from the 11th stage of the compressor in Smith's paper, shown in Figure 13.

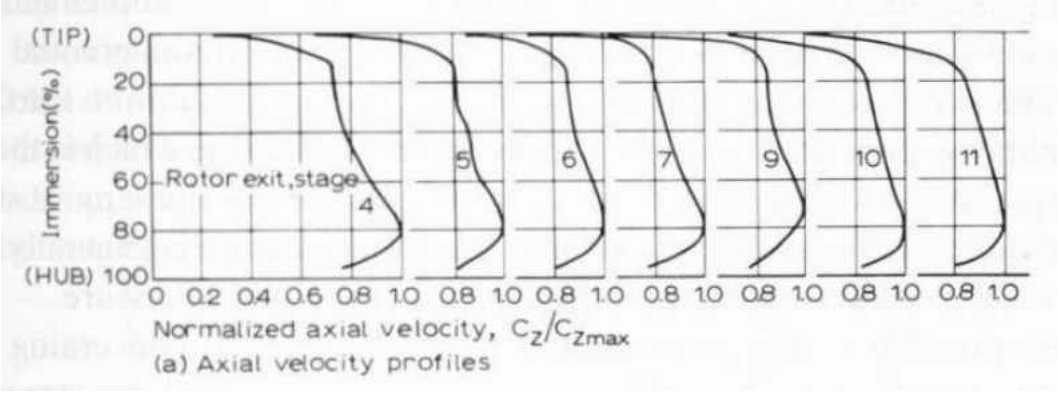

Figure 13: Stage 11 Velocity Profile

The second velocity profile used for this evaluation was from the 4th stage of the presented compressor, shown in Figure 14. This profile was chosen for its complexity compared to that of the 11th stage velocity profile

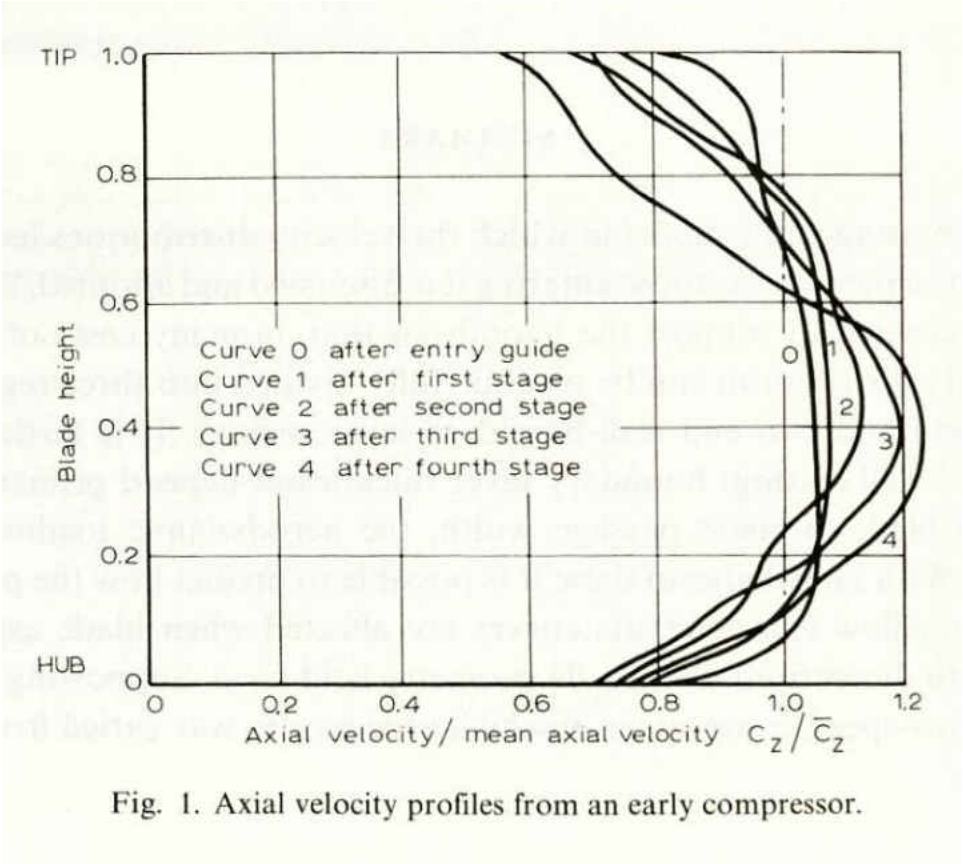

Fig. 1. Axial velocity profiles from an early compressor.

Figure 14: Compressor Stage 4 Velocity Profile

With the velocity profiles selected for testing the methodology previously presented was used to design an annular velocity profile generating screen for each of the desired velocity profiles. The number of separate annular sections selected for this test was 3 for the 11th stage velocity profile and both 3 and 5 sections for the 4th stage velocity profile. Figure 5 shows a representation of an annular screen divided into 3 sections of varying solidity for clarity. The 4th stage velocity profile was chosen to have multiple screens designs tested because of its complexity to also evaluate the accuracy achieved with the added screen sections.

The first screen tested was the screen designed to simulate the velocity profile at the 11th stage of the compressor presented by Smith. The reference velocity profile, the predicted profile based on the 3 section screen design, and the test data including error bars is shown in Figure 15. The velocity measured is non-dimensionalized by the maximum velocity and the radial positon is non-dimensionalized so that the origin represents the hub (bottom) and 1 represents the tip (top) of the annular section. The relative uncertainty associated with this non-dimensional velocity analysis is on the order of 4%.

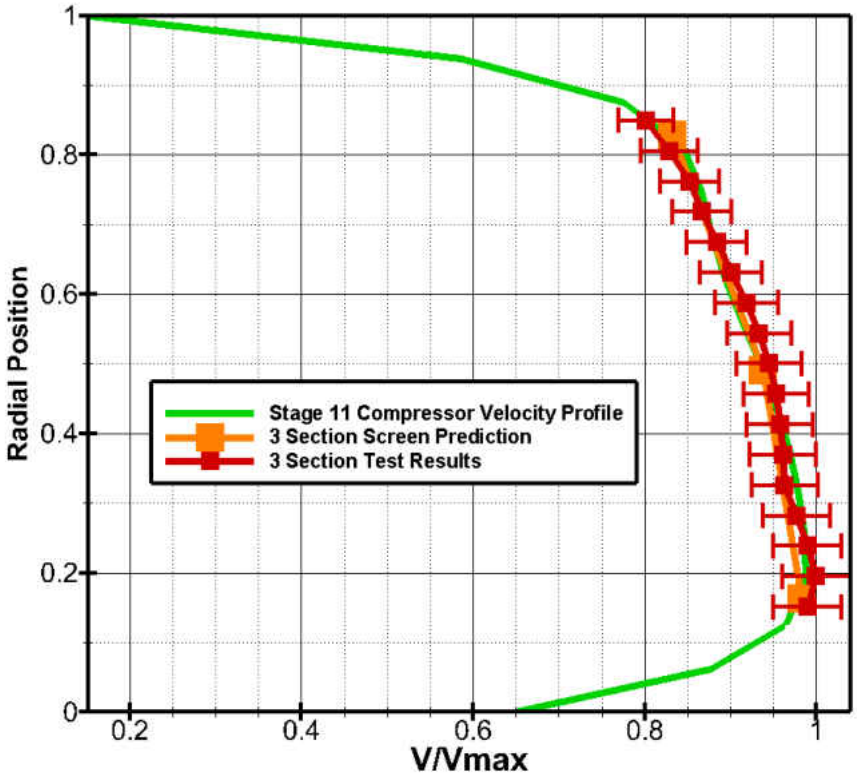

Figure 15: Stage 11 Velocity Profile Test Results

The screen produced an accurate representation of the desired velocity profile. In an effort to quantify the accuracy of the fitment of the measured velocity profile to that of the supplied velocity profile a value of the mean absolute error will be used, shown in Equation (8).

$$MAE = \frac{1}{n}\sum_{i=1}^{n}\left|x_{measured} - x_{reference}\right| \quad \textbf{(8)}$$

Mean Absolute Error

For consistency, the measured and reference velocity profile is non-dimensionalized by the maximum axial velocity. The velocity profile tested to simulate the 11th stage of a compressor produced a mean absolute error of only 0.009.

The next velocity profile to be tested was the profile that simulated the 4th stage of a compressor. The first data set presented is from the screen with the 3 section design shown in Figure 16.

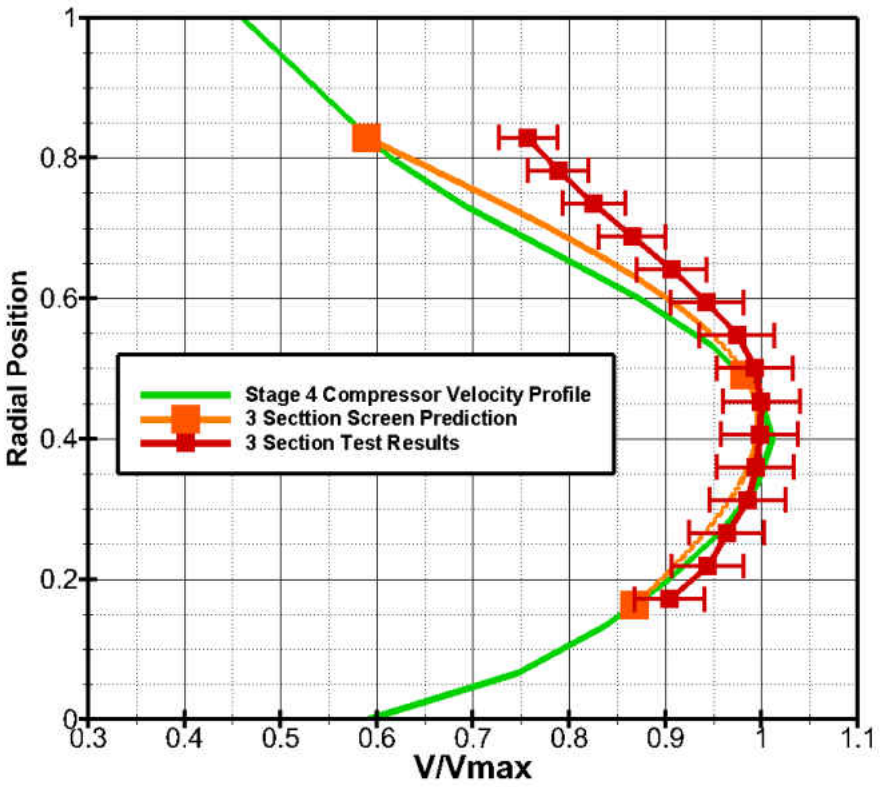

Figure 16: Stage 4 (3 Section) Velocity Profile Test Results

The test conducted for the 3 section screen design for the 4th stage velocity profile produced a mean absolute error of 0.0653. This velocity profile was not as good of a match compared to the 11th stage velocity profile generating screen, but did offer some insight into a problem faced by the current design. The tip side of the velocity profile, towards 1 in the radial position, shows a deviation from the predicted velocity profile in the area of the steepest velocity gradient. The velocity profile generating screens appears to have a limit to the velocity gradient that can be achieved. This could be related to a limitation in change of porosity from one section to the next or it could be related a limit in velocity-porosity predictability. The porosity change between the

top two sections is approximately 0.193 which equates to a velocity ratio of 0.725. The section closest to the tip side approaches the solidity limit perceived by Castro and Villermaux where instabilities start to occur. The limit perceived by Castro and Villermaux is approximately 0.5 and the final section in this screen has a solidity of 0.49.

The next screen tested was the 5 section screen design used to produce the 4th stage velocity profile shown in Figure 17.

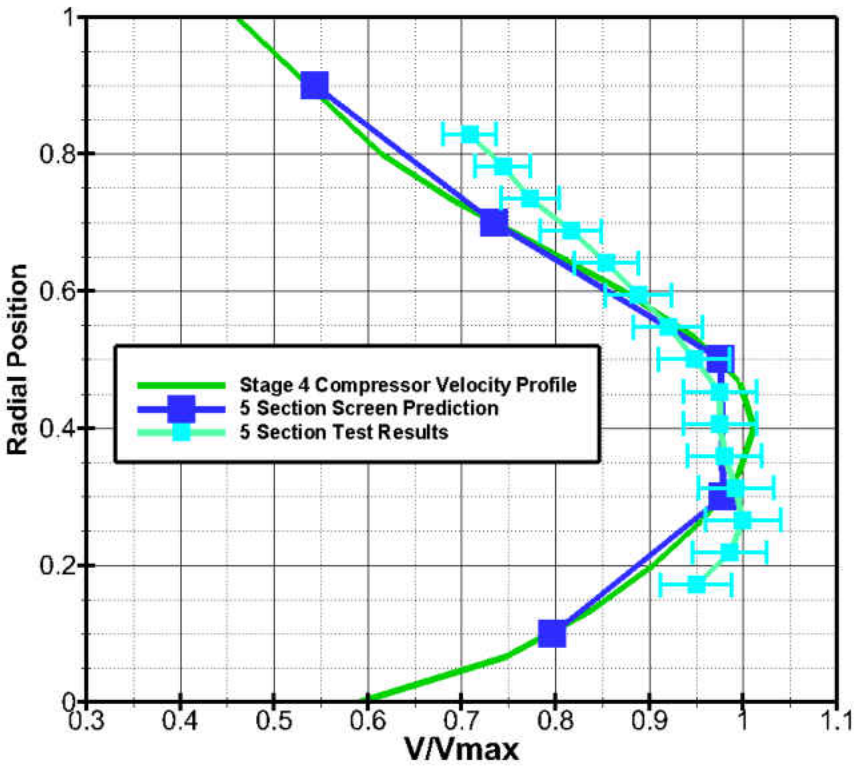

Figure 17: Stage 4 (5 Section) Velocity Profile Test Results

This velocity profile generated by the 5 section velocity profile generating screen produced a profile with a mean absolute error of 0.050. This mean absolute error is less than that of the 3 section design, but also offers some other insights. The same velocity gradient issue appears to be present on the tip side of the profile. This screen does not have as large of a porosity change as that seen in the 3 section design, but does have a section, closest to the top, that has a porosity that is close to the range of instability. The largest porosity change is 0.114 between the top two sections and the highest solidity is 0.52. The other observation that can gleaned from this data set is that placement of the screen sections appears to be more important than just the pure increase in the number of sections for added accuracy. These baseline tests give us some information about the area of concerns in the design of the screens that can be of focus in the third experiment.

Experiment 2

The trends of all the screens tested in this experiment were similar, so for the review of the overall data set, Screen 1 has been chosen as a representative case. The first step in the analysis was to identify the different regions of jet development in relation to the streamwise distanced downstream of the perforated plate. There are two main criteria that help to identify these regions, the centerline jet velocity and the skewness of the velocity. Mohamed and Larue provided (Mohamed & Larue, 1990) a methodology to identify the isotropic turbulence region by using the skewness of the velocity, shown in Equation (9). Skewness is used to evaluate the symmetry of a population compared to its mean value. A positive skewness means that velocity

is more likely to take on a larger value compared to the mean and vice-versa for negative skewness. In a region of locally isotropic turbulence the velocity skewness approaches zero. A criterion to identify where the skewness is approximately zero is to use twice the standard error of the skewness as the limit. Once the skewness passes this limit and the change in jet centerline velocity is also approximately zero the flow is assumed to be in the region of homogeneity.

$$velocity\ skewness = \frac{\overline{v'^3}}{\left(v'^2\right)^{\frac{3}{2}}} \tag{9}$$

Velocity Skewness

$$\boldsymbol{skewness\ error\ \approx\ \sqrt{\frac{6}{sample\ size}}} \tag{10}$$

Skewness Error

In Figure 18 the jet velocity decay and velocity skewness are shown. The velocity skewness, as mentioned above, gives an indication of where the flow approaches locally isotropic turbulence. At the fourth position downstream of the screen, at x/M approximately 7, the velocity skewness is below the limit. The other criterion for a velocity profile to be complete is when the change in velocity is approximately zero for all the screens tested. This is show to happen at approximately 11 mesh lengths downstream of the screen. This analysis provides us with a condensed region for analysis of the mixing region and gives a distance that can be compared to other screens in terms of how long it takes for the flow to become homogeneous.

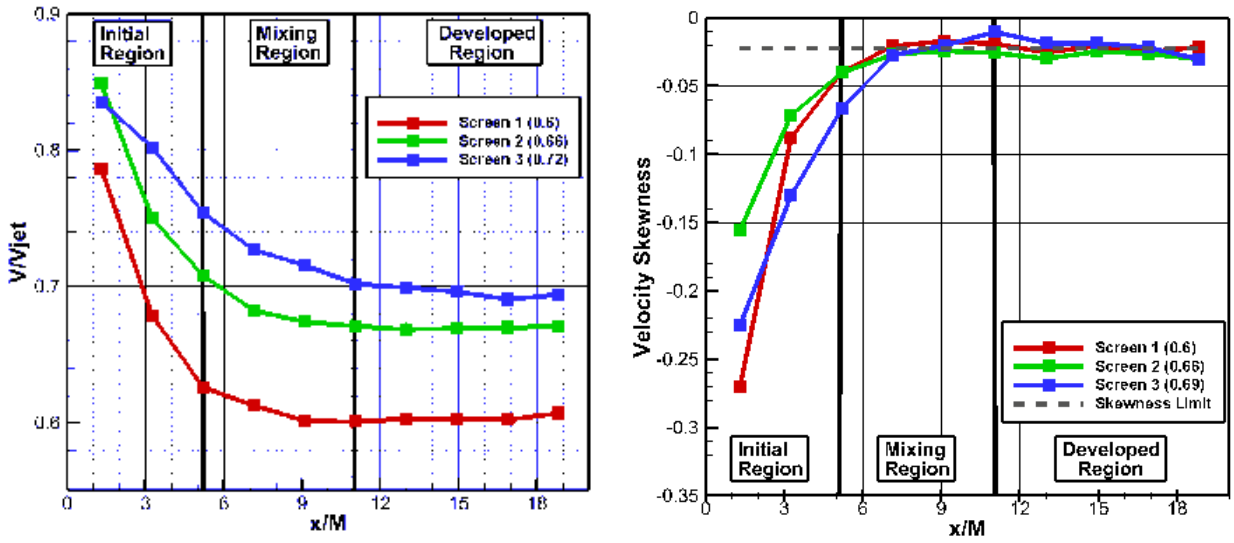

Figure 18: Jet Velocity Decay (left) and Velocity Skewness (right)

After using the skewness and centerline velocity trend to identify the region where turbulence is essentially isotropic, one more trend can be identified before moving forward with the analysis. One of the ways to characterize the bulk motion of fluid is to identify trends in centerline jet velocity. Making an assumption to describe the decay of velocity in the streamwise direction of the flow is one way to simplify a complex flow system. Gran Olsson theoretically and experimentally described the flow behind a mesh screen in a detailed manor by simplifying the jet centerline velocity decay (Schlichting, 1979). Olsson described the flow past a mesh screen as a wake through a cascade of cylindrical bodies, shown in Figure 19. Olsson described the damping of the bulk velocity variations by assuming that the decay of the velocity was proportional to $\frac{1}{x}$ after an initial region. This assumption is also used to describe circular

turbulent jets. Other simplifications include describing the decay of velocity for a two dimensional wake as being proportional to $\frac{1}{\sqrt{x}}$ (Schlichting, 1979).

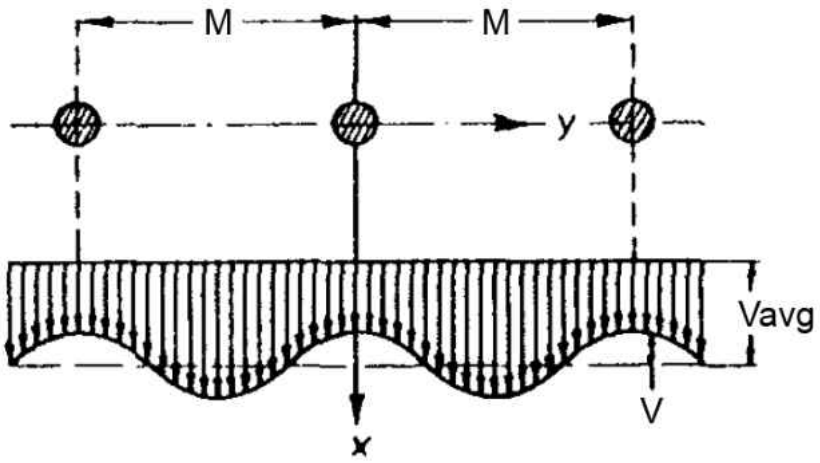

Figure 19: Wake Past A Cascade of Cylinders

With this relationship identified a look back at Figure 18 will shed more light on the interactions in the flow in the remaining region, the Initial or Near Field Region. In the beginning of the flow, until approximately x/M=5, the velocity of the jets decay in a linear manor similar to that of an axisymmetric jet. This allows us to identify the Near Field Region into where the fluid acts similarly to that of independent jets. The independent jets spread until they meet and interact with each other in the Mixing Region. The axisymmetric jet region can be described by the velocity decay being proportional to $\frac{1}{x}$ while the mixing region will require a more complex equation to describe its decay.

With the understanding of the regions of interest, the velocity obtained in testing Screen 1 is shown in Figure 20. In this data the most apparent trend is the reduction in the overall bulk variation of velocity as the flow propagates downstream, shown from left to right.

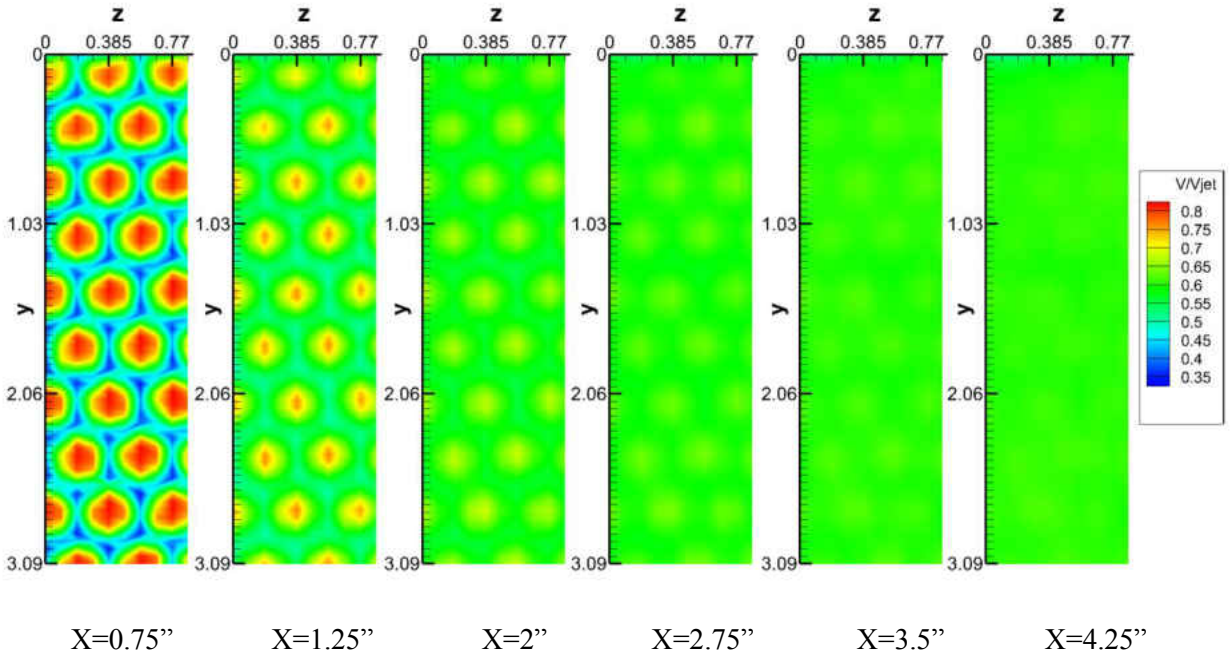

Figure 20: Screen 1 Non-Dimensional Velocity Data (moving downstream from left to right)

This decay term helps to describe the decrease in the overall bulk velocity variation originally produced by the perforated plate. This velocity decay in the mixing region can be described by a power law function presented in the research done by Mohamed (Mohamed & Larue, 1990). In this region the centerline velocity decay of the jets can be described by the power law decay function listed in Equation (11).

$$u(x) = A * \left(\frac{x}{M}\right)^{-n} + V_O \tag{11}$$

Jet Centerline Velocity Decay

The function listed in Equation (11) uses a non-dimensional term to describe the position downstream of the screen. This term, x/M, is the x position divided by the mesh width, M, and is adopted to remain comparable to wire mesh screens. The data collected in this experiment included data that extended from the center of the test section to the top wall, the Y origin in the previously mentioned local coordinate system. The data set used in the evaluation of the jet centerline velocity decay was taken at a distance far enough from the wall that the viscous affects from the wall were negligible.

In the evaluation of this data set, an average centerline jet velocity at each downstream plane was taken and non-dimensionalized in two different ways. The first term used for the non-dimensional analysis was the maximum jet velocity. This maximum jet velocity is achieved at the exit of the perforated plate and is different for each specific plate. This non-dimensional evaluation is shown in Figure 21. The decay rate obtained provides a way to see how much velocity decay increases with solidity.

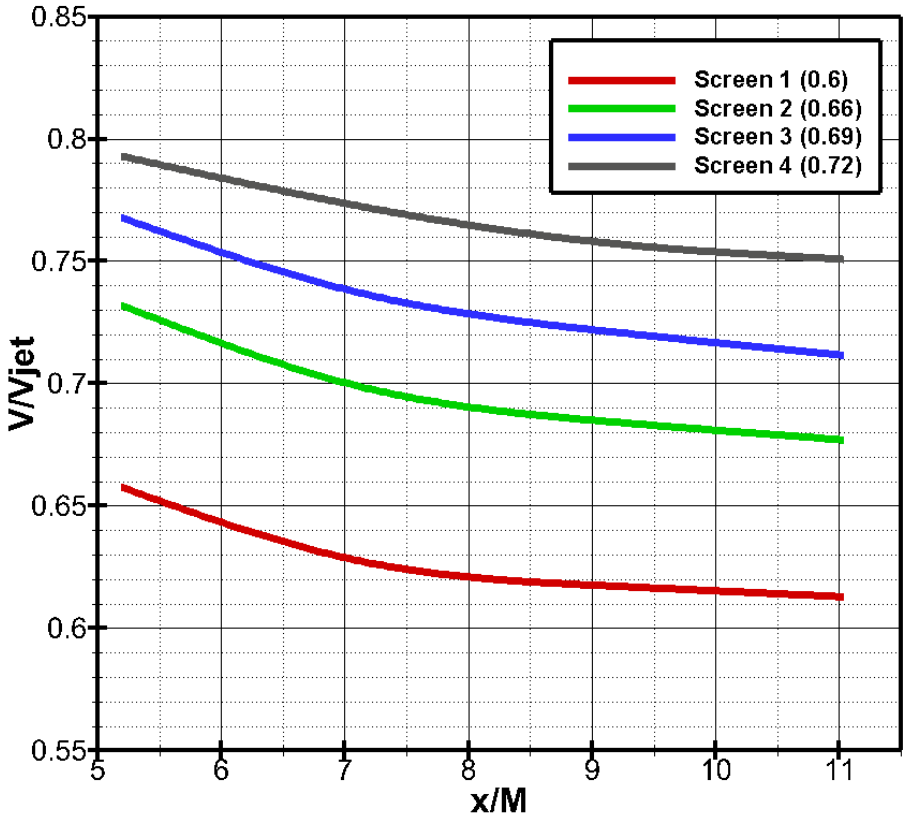

Figure 21: Non-Dimensional comparison of (Velocity/ Exit Velocity of Jet) and (x position/mesh width)

Table 5: Power Law Decay coefficients for Non-Dimensional analysis of (Velocity/ Jet Exit Velocity) and (x position/mesh width)

	A	n	V_o
Screen 1	5.677	2.866	0.6072
Screen 2	1.964	2.023	0.6619
Screen 3	0.8144	1.354	0.6802
Screen 4	0.3778	0.8868	0.7055

There are two observations that can be made from this data set. The jet velocity decays to a mean - jet maximum velocity ratio that is proportional to the porosity. The other observation that can

be made is that the velocity decay exponent, n, has a linear relationship to the porosity. This can be seen in Figure 22.

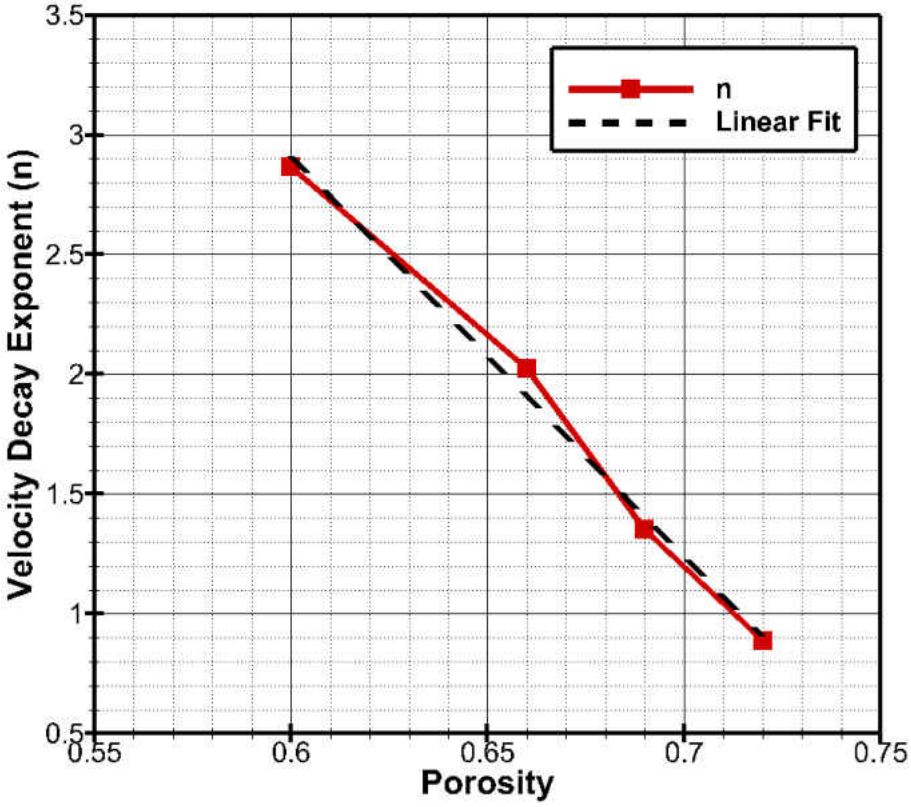

Figure 22: Decay Exponent vs Porosity

The next term used for non-dimensional analysis is the average fluid velocity at each plane. Results of this analysis are show in Figure 23 and Figure 24 with the power law coefficients shown in Table 6. This data set helps to show that with the increase in centerline velocity decay and exit jet velocity associated is proportional to the increase in solidity. This proportionality can be seen in the behavior of the bulk flow downstream of the screen, approximately x/M=11,

where the bulk velocity fluctuations start to converge towards the average. The bulk fluctuations decay towards zero so that the jet centerline velocity approaches the average velocity at approximately the same distance downstream of the perforated plate. This mean that for all the plates tested the centerline jet velocity decay can be described using a single function, shown in Figure 24, similar to what was used by Olsson.

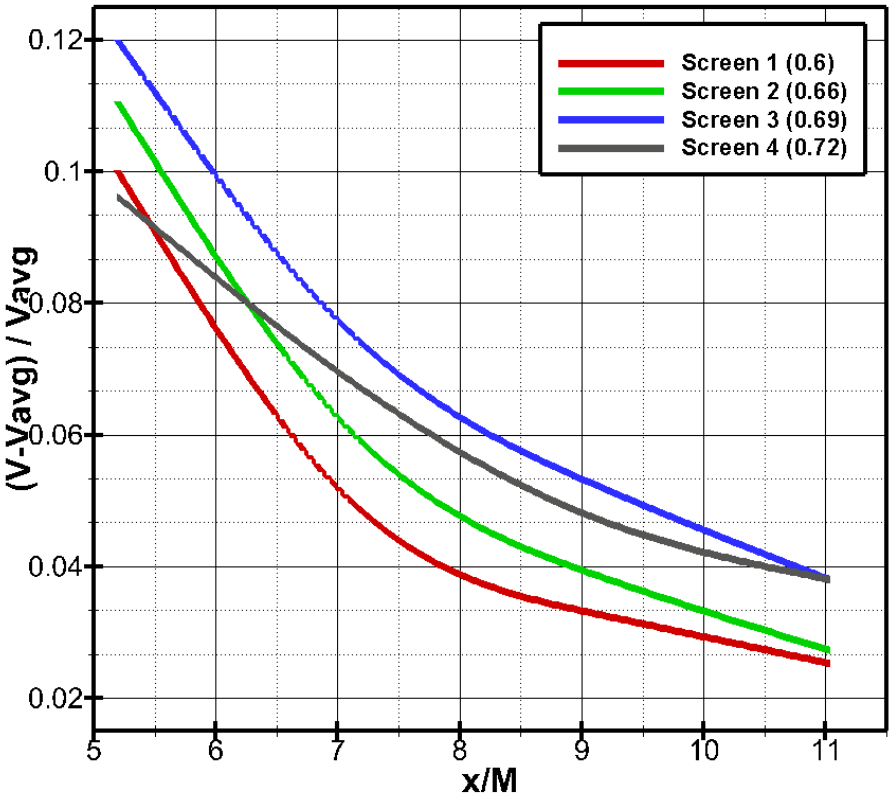

Figure 23: Non-Dimensional comparison of (Velocity/ Average Velocity) and (x position/mesh width)

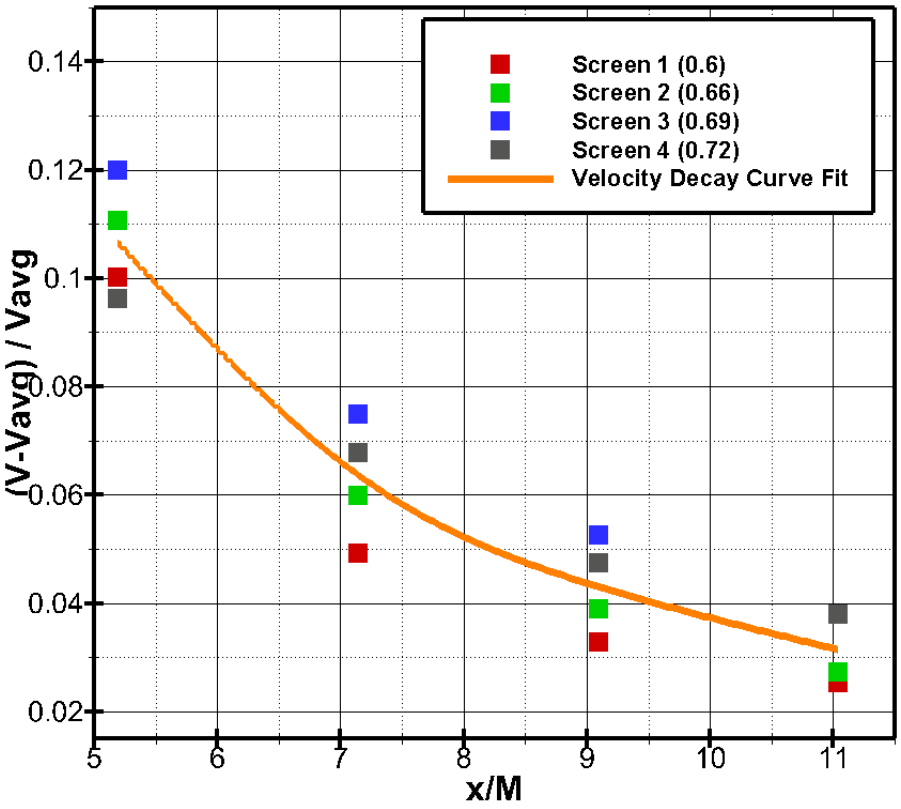

Figure 24: Curve fit for Non-Dimensional comparison of (Velocity/ Average Velocity) and (x position/mesh width)

Table 6: Power Law Decay coefficients for Non-Dimensional analysis of (Velocity/ Average Velocity) and (x position/mesh width)

	A	n
All	2.609	1.985

The analysis of the jet centerline decay is a good way to better understand the bulk motion of the fluid, but to better understand the mixing of jets an analysis similar to that done for the jet

centerline velocity is applied to the turbulent intensity of the shear layer between the jets. Figure 25 shows the decay of the turbulent intensity as the fluid moves downstream of the screen, from left to right.

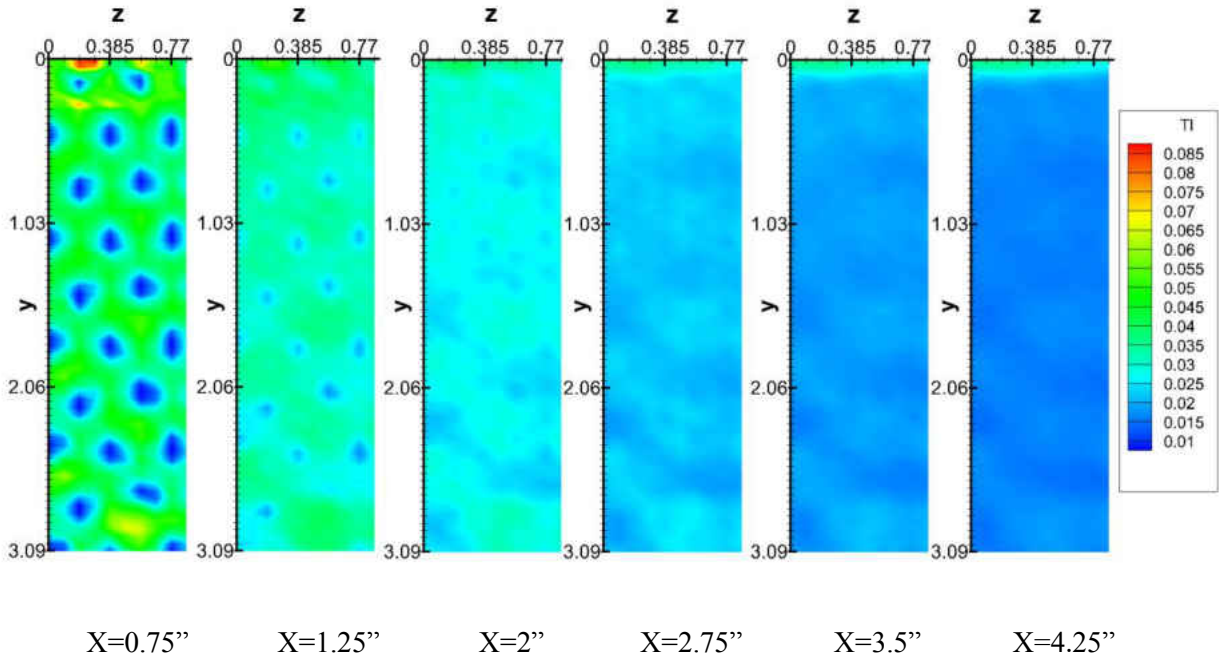

Figure 25: Screen 1 Turbulent Intensity Data (moving downstream from left to right)

The same criteria used in the centerline jet velocity analysis depicting where the decay power law holds true can be applied. Figure 26 shows the decay of the turbulent intensity, for each screen, compared to the downstream position. The distance downstream of the screen is non-dimensionalized by the jet diameter for comparison to similar data.

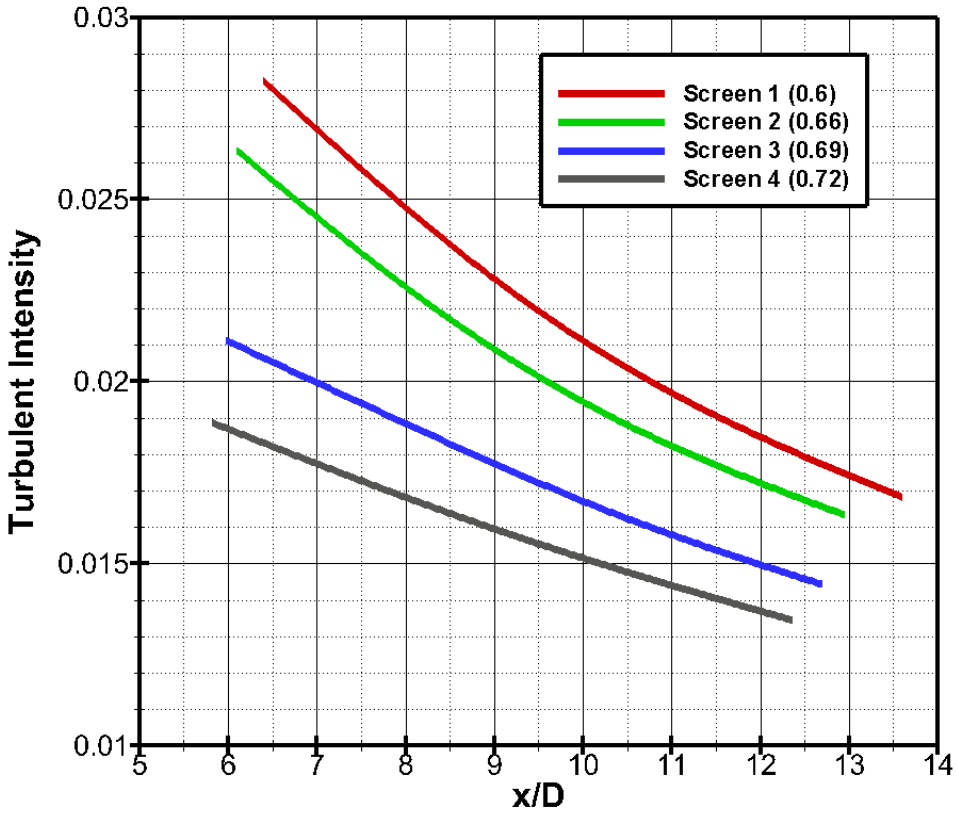

Figure 26: Non-Dimensional comparison of (Average Turbulent Intensity) and (x position/hole diameter)

The power law decay function for the turbulent intensity did not require the inclusion of a virtual origin to provide an accurate fit and was omitted in the data provided in Table 7. The results obtained here are on the same order of those obtained by Roach in his investigation of turbulent intensity decay in perforated plates (Roach, 1987).

Table 7: Power Law Coefficients for Non-Dimensional Comparison of (Turbulent Intensity at the Jet Shear Layer) and (x position/hole diameter)

	A	n
Screen 1	0.0886	0.689
Screen 2	0.0756	0.636
Screen 3	0.0492	0.505
Screen 4	0.0399	0.447

The last term used for characterization of the Mixing Region of the perforated plate flow, is variance. The variance is a term used to describe how much, on average, the flow deviates from its average. This term is the focus of comparison in the work of Mohamed and Larue (Mohamed & Larue, 1990). The solidities of the mesh screens in the data sets collected by Mohamed and Larue are in the range as Screen 1 and 2.

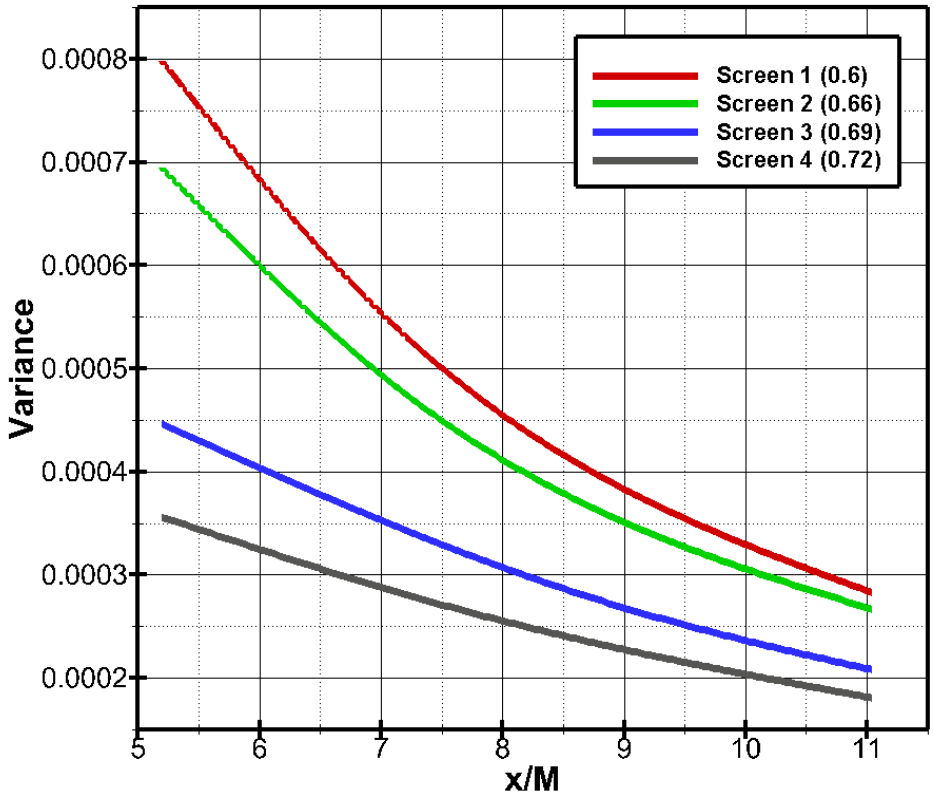

Figure 27: Non-Dimensional comparison of (Variance) and (x position/mesh width)

Table 8: Power Law Coefficients for Non-Dimensional Analysis of (Turbulent Intensity at the Jet Shear Layer) and (x position/mesh width)

	A	n
Screen 1	0.00701	1.318
Screen 2	0.0052	1.223
Screen 3	0.002	0.913
Screen 4	0.0013	0.813

The decay rate of the variance obtained is very similar to that from Mohamed. The power decay term, n, they obtained is on the order of 1.24-1.33.

Experiment 3

The data set from Experiment 2 provides a baseline for comparison to a more complex interaction involving screens of different solidities. This data set aims to characterize the interaction between perforated plat sections of different solidities. The characterization used in this experiment is based on the criteria used in a classification of turbulence study referred to herein as plane layer mixing. In plane layer mixing experiments two streams of uniform velocity interact with each other to form a discontinuity that mixes out in a predicable manner. Figure 28 uses a graphic to visualize the discontinuity obtained at the end of a splitter plate, left, and the mixed velocity profile obtained downstream on the right. The mixing layer linear growth is visualized by using red line to signify the edges of the mixing layer.

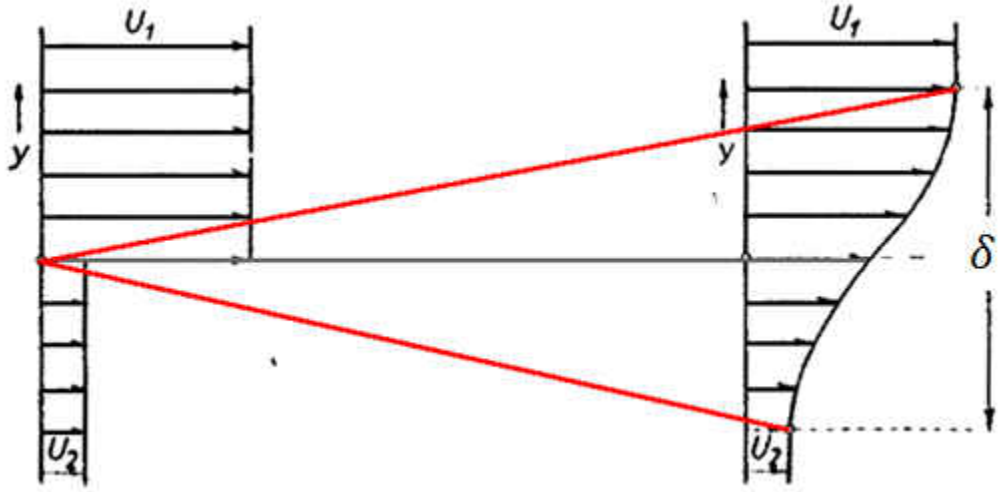

Figure 28: Plane Layer Mixing

The mixing layer can be characterized using a few terms. These terms include the mixing layers width (δ), the spreading rate $\left(\frac{d\delta}{dx}\right)$, mixing layer centerline offset, (Y_o), and free stream velocity (U_2 and U_1) . The mixing layer is a turbulent flow that forms between the two uniform free stream velocities. The width of this turbulent layer is described by δ. This mixing layer expands into the uniform velocity profile in a linear fashion proportion to the streamwise direction and is characterized by the spreading rate. As the flow propagates downstream the mixing layer is not always going to be centered along the original velocity discontinuity plane. The mixing layer spreads in a linear fashion, but the center of the mixing layer will also shift, or be entrained, in a linear fashion which will be characterized by its dimensional offset Y_o. With the parameters to be identified presented, an example of the data set can be seen in Figure 29. This data set is taken from Screen 7 and will be used as a representative case in this analysis.

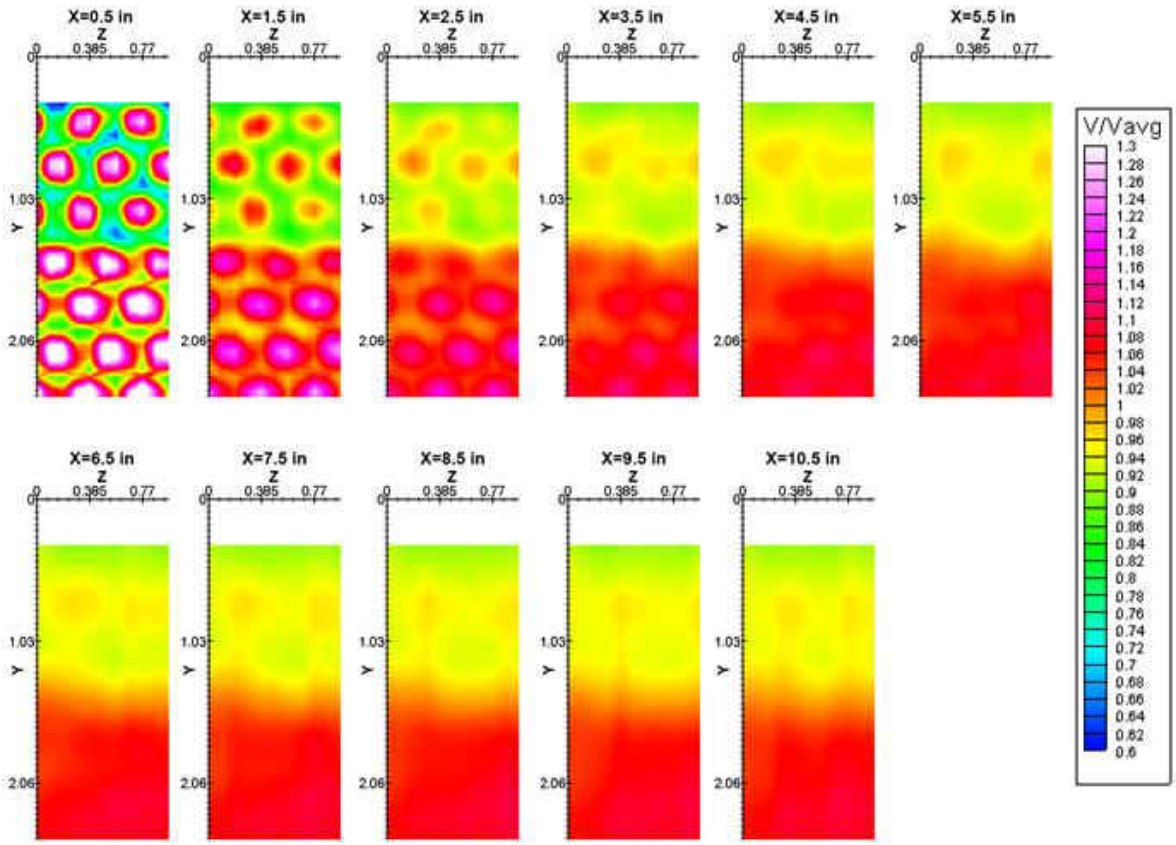

Figure 29: Screen 7 (0.09) Velocity

The area of interest for this investigation includes the two rows of jets above and below the velocity discontinuity plane. These jets above and below the discontinuity plane represent two sections of perforated plate that would be used in a velocity profile generating screen to match specific velocities. The location of interest is shown below in Figure 30. For this analysis the velocity discontinuity plane will be set as the Y origin. The perforated plate section of higher porosity and higher velocity, corresponding to U_1, is in the positive Y direction. The perforated plate section of lower porosity and lower velocity, U_2, is in the negative direction.

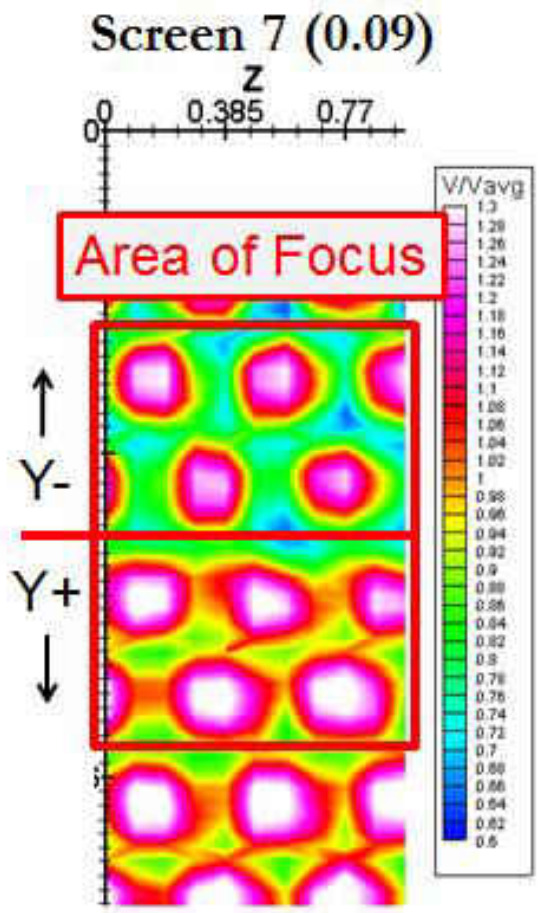

Figure 30: Screen 7 (0.09) Jets of Interest

The data collection was started offset the wall and any obvious wall effects are negligible in the area of interest. A few observations can be made that are consistent between each of the data sets. One initial observation that can be made is the fluid reaches a self-similar state at approximately 5.5", or x/M=14.29", downstream of the perforated plate. This is clearer when taking an average of the velocity in the Z direction, as can be seen in Figure 31. The velocity profile obtained through this averaging shows that the velocity profile that remains is virtually unchanged after this distance downstream of the perforated plate.

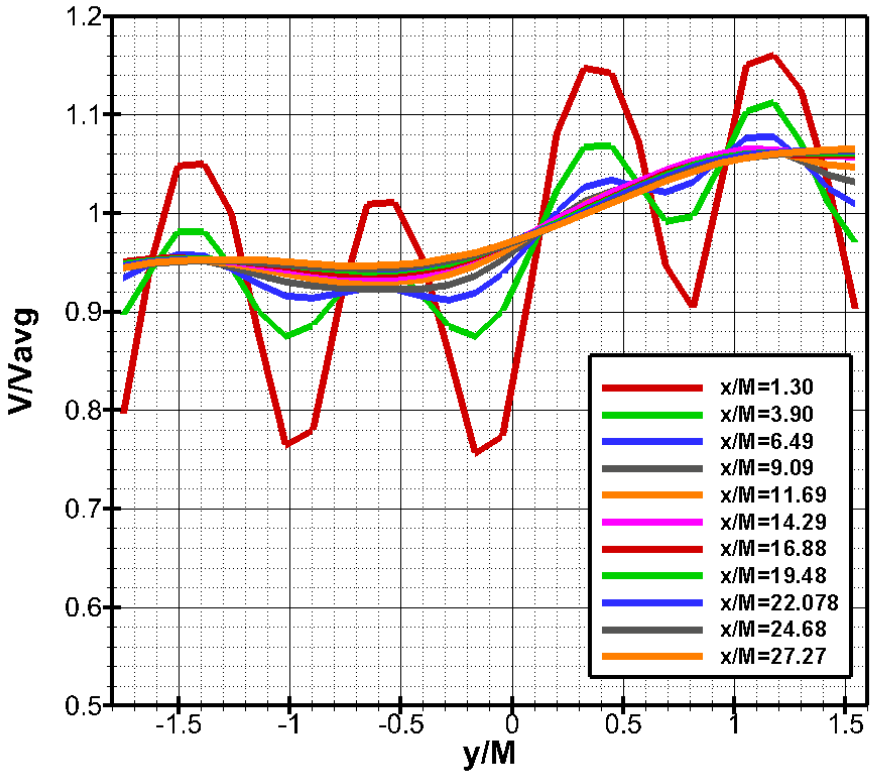

Figure 31: Screen 7 Average Velocity Data

This observation coincides with the identification of the Developed Region in the evaluation of the single solidity screens in Experiment 2. The identification of this region is important to define the range where the desired velocity profile can be considered fully developed. The identification of this range is also important because it is this range that the identification of the parameters for plane layer mixing will be the most apparent and provide usable data.

With the range identified for useable data, a methodology for evaluation is presented which will include a non-dimensional analysis. This evaluation methodology relies on the idea that the plane

mixing layer produced by the perforated plates of different solidities is an asymmetrical self-preserving free turbulent flow. Self-preservation occurs when velocity profiles or other quantities can be made to be self-similar when scaled by a local velocity scale. The normalizing velocity scale chosen is shown in Equation (12).

$$U^* = \frac{U - U_2}{U_2 - U_1} = \frac{1}{2} * \left(1 + erf\left(\frac{Y - Y_o}{\delta}\right)\right) \quad \textbf{(12)}$$

Local Velocity Scale

This local velocity scale was presented by Townsend (Townsend, 1976) and is used in analysis by other researchers such as Mehta (Mehta, 1991). The derivation of this equation will not be presented in this investigation, but the main assumptions made include constant eddy viscosity and an assumption of symmetry. This scaling factor incorporates all of the parameters mentioned earlier and will be used to characterize the plane mixing layer data in the Developed Region. The values for the mixing layer width and centerline offset were obtained through a curve fitting process where the local maximum and minimum were obtained from the area of interest and used for the U_2 and U_1 variable respectively. In an effort to evaluate this methodology, the goodness of fit of this relationship to the data for all of the screens tested was monitored. All of the data sets in the Developed Region fit well and had an R^2 in excess of 0.99. The local velocity scale for Screen 7 is shown plotted against the similarity coordinate in Figure 32. The similarity coordinate is included in the error function and contains the centerline offset and mixing layer width.

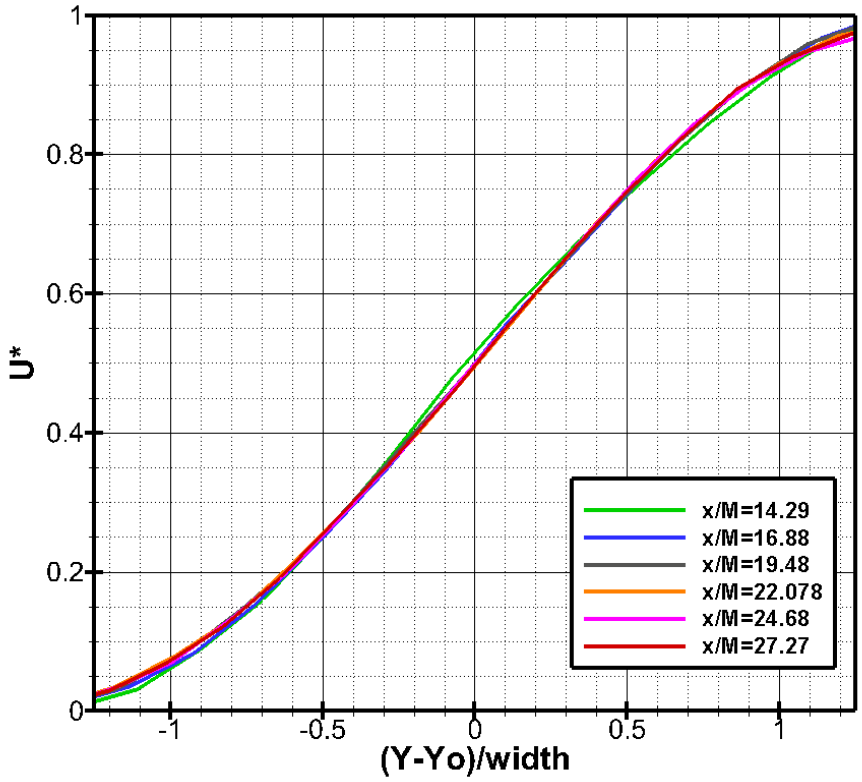

Figure 32: Local Velocity Scale vs Similarity Coordinate for Screen 7 (0.09)

A criteria used in the evaluation of the single solidity screens was the skewness value. This value was used to identify when the flow entered a region that could be considered locally isotropic. It can be observed in the evaluation of the mixed solidity screens that after an initial region, which ends at around x/M=6.5, the flow in the regions outside of the mixing layer trend towards homogeneity. This trend is consistent with that of a single solidity screen or a flow lacking a significant velocity gradient. A plot of skewness at different streamwise locations downstream of the perforated plate tested is shown in Figure 33.

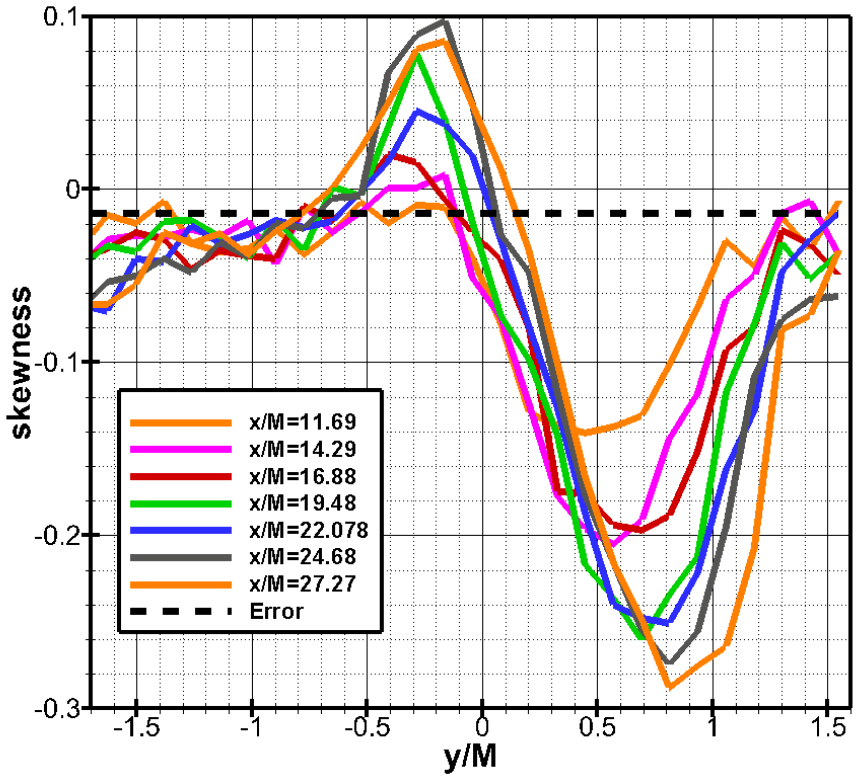

Figure 33: Screen 7 (0.09) Skewness

Skewness can also be used in the evaluation of the mixed solidity screens in a different manner. Skewness will have a maximum and minimum at the edges of the mixing layer. This location obtained from the maximum and minimum skewness can be used to verify the location of the edges of the mixing layer obtained from error function parameters. Both of these parameters grew in a linear manner with respect to the streamwise direction downstream of the perforated plate tested. This trend follows the expected trend observed in plane mixing layers and is shown in Figure 34.

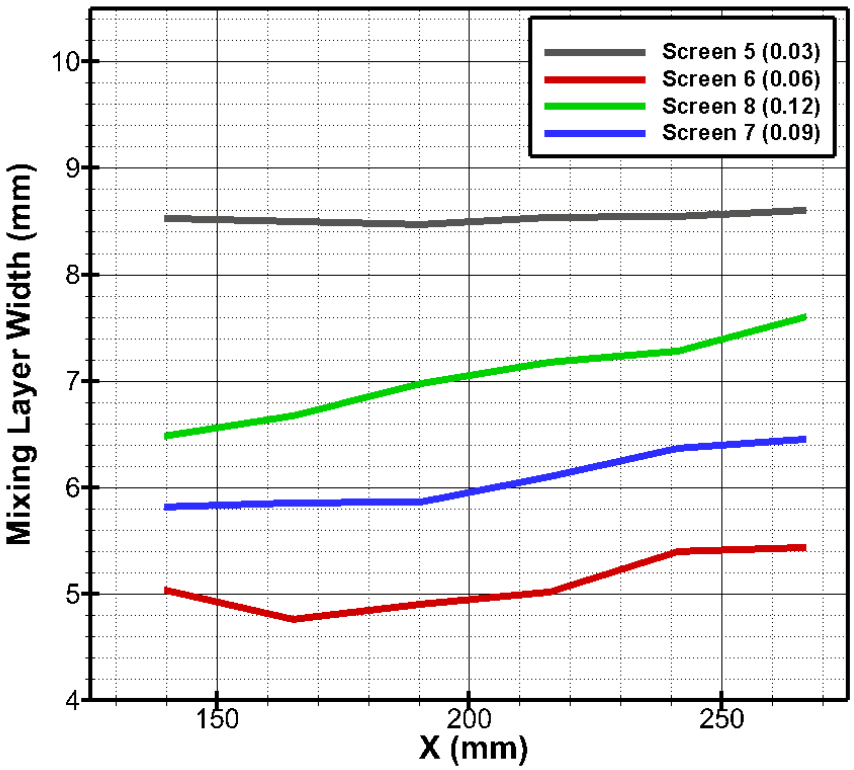

Figure 34: Mixing Layer Width (δ) vs Streamwise Distance

The trend that can be observed from this data set is that with an increase in difference in porosity, or decrease in velocity ratio, the slope for the streamwise distance - mixing layer width correlation increases. This slope is the spreading rate and can be seen in Figure 35.

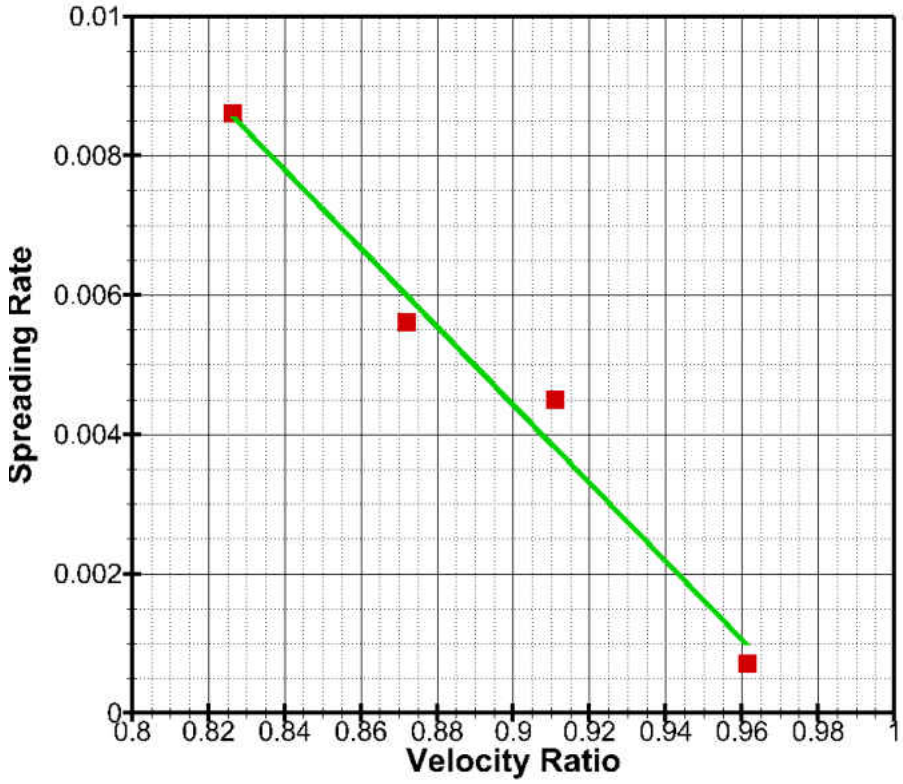

Figure 35: Spreading Rate vs Velocity Ratio

This linear trend agrees with those obtained by other researchers in the area of plane layer mixing. A few other observations can be obtained from this data set. One of the most significant is the mixing layer width compared to that of the area of interest. For all the cases tested the width of the mixing layer is smaller than that of the two different solidity sections combined which allows a prediction of the free stream velocity, U_2 and U_1, based on the outer most jets velocity.

The evaluation of the free stream velocity for the plane mixing layer theory is conducted in the same manner that was used in the evaluation of the centerline velocity jet decay in the single solidity test. The rows of the outer most jets, in the area of interest, are the jets to be evaluated.

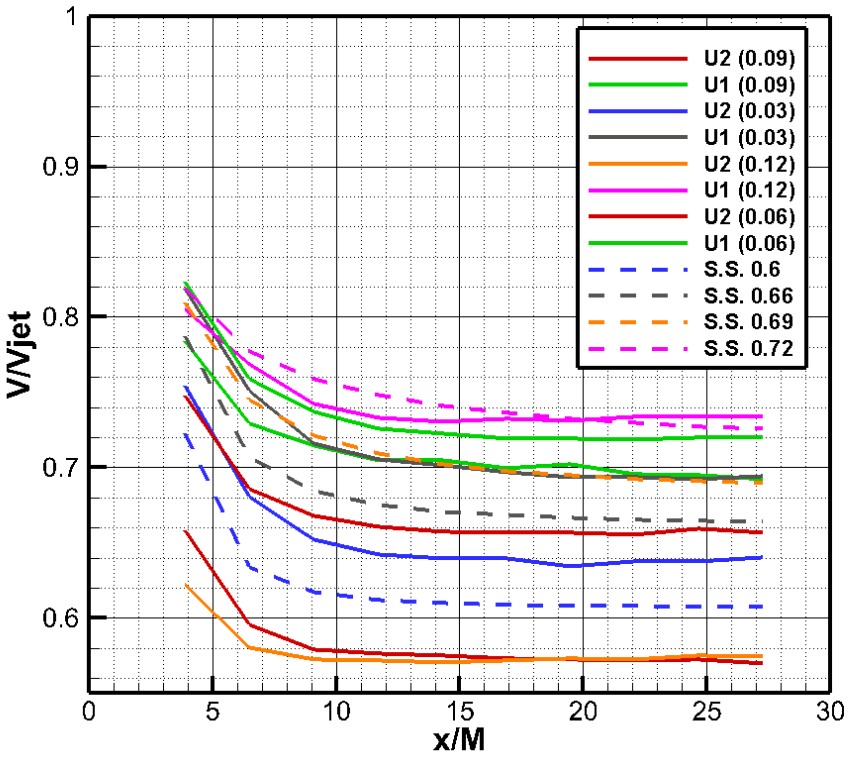

Figure 36: Free Stream Jet Velocity Decay

This data set shows the free stream velocity obtained from all the mixed porosities as well as single solidity case for reference. The higher velocities of the mixed solidity cases, U_1, match well with the velocities obtained from the single solidity cases. This shows that these previously obtained correlations will work well as a prediction. The lower velocities of the mixed solidity cases, U_2, appear to not match as well to their reference single solidity cases. Upon examination

with the inclusion of uncertainty, shown in Figure 37, the values are within a range of predictability using the previously obtain correlations. For this non-dimensional analysis the relative uncertainty is on the order of 6%.

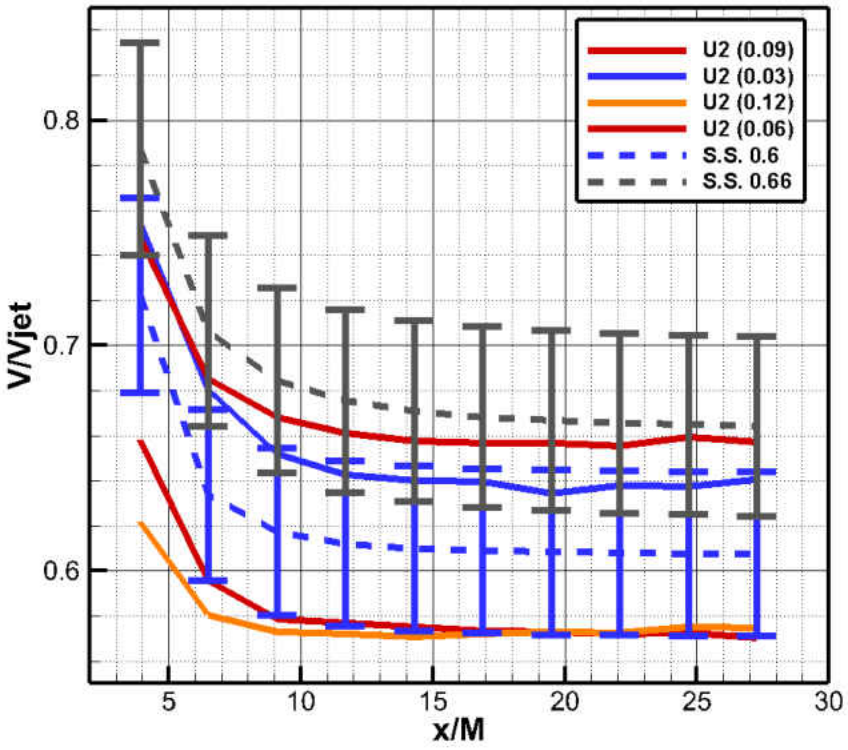

Figure 37: Mixed Solidity Lower Velocity with Uncertainty

More insight into the reasoning as to why the lower free stream velocity does not match as well to that of the previously obtained correlations can be obtained when evaluating the mixing layer centerline offset.

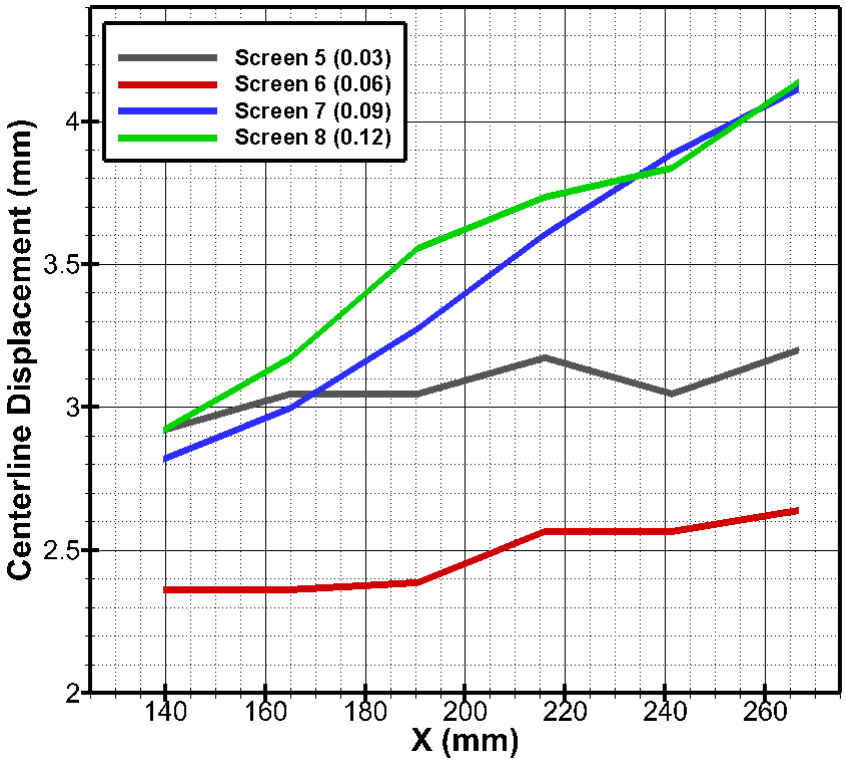

Figure 38: Mixing Layer Centerline Offset

From the data a few trends can be observed. The shifting of the centerline is in the direction of the high velocity which is also the direction of lower turbulent intensity. This trend is different than that previously observed since the shift is normally in the direction of lower velocity. This trend does back up the observation seen in the free stream velocity decay in that mass transfer from the lower velocity side to the higher velocity side would offset the velocity decay from that previously obtained in the single solidity tests. This can be attributed to the difference in turbulent intensities, shown in Figure 39.

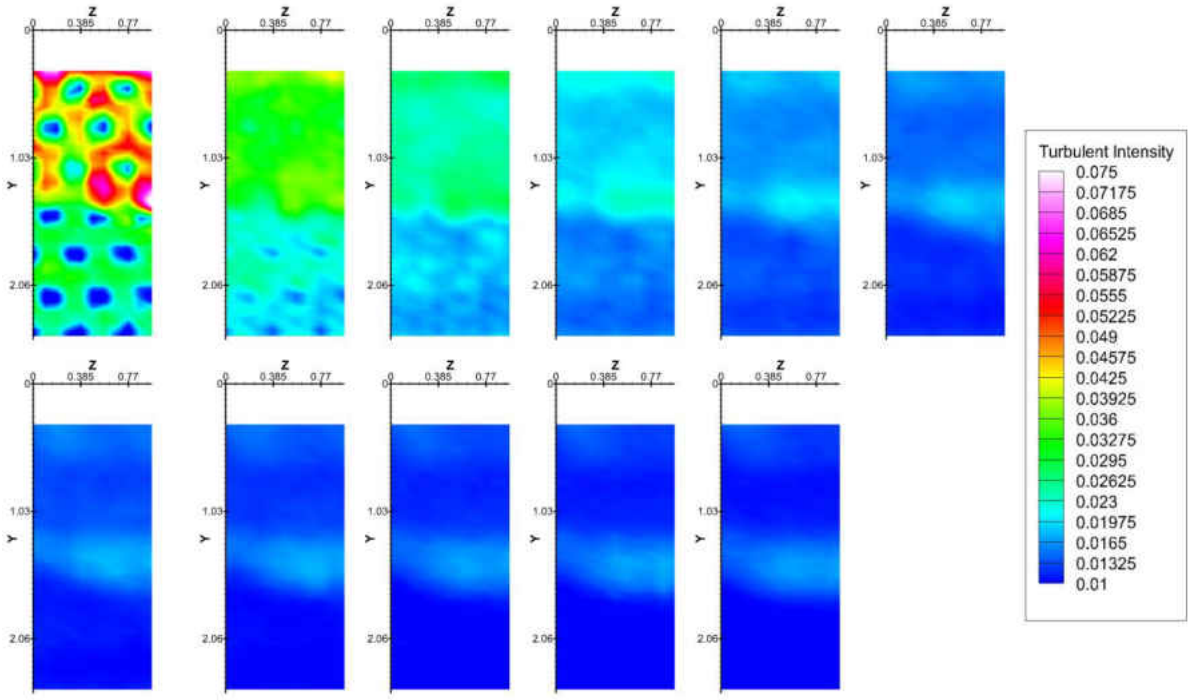

Figure 39: Screen 7 (0.09) Turbulent Intensity Data

A correlation for the mixing layer centerline compared to velocity ratio was not obtained in the investigation and will be reserved for future investigations.

CHAPTER FIVE: CONCULSION

The screen design presented in this paper to match velocity profiles for testing of gas turbine components provided a reasonable match for the tested inlet condition. The absolute mean error obtained in the testing of specific velocity profile generating screens ranged from 0.009-0.065. The relative uncertainty associated with the measurements is 4% so there is room for improvement. In the testing of a sample set of screens the error that exceeded the relative uncertainty was observed in locations of larger velocity gradients. The tests conducted aimed to identify the source of the issue.

The single solidity tests conducted analyzed the interaction of the jets/wakes produced by the perforated plates and provided data that will improve future designs of the velocity profile generation screen. There are a few conclusions that can be made when comparing the results of perforated plate test to those previously conducted. The decay rate of the centerline jet velocity in the initial region is linear in nature, but is not as rapid as that of an axisymmetric turbulent jet. The decay rate of the centerline jet velocity in the mixing region is of the same order or greater than that in the initial region. The decay rate is this region was shown to increase with solidity in a linear fashion. The bulk fluctuations of the flow damped out at approximately the same distance from the perforated plate for all the solidities tested. This transition to a region of isotropic turbulence was faster than that obtained for wire mesh screens, $x/M > 30$, and faster than that of perforated plates tested previously by Liu, $x/M=17$ (Liu, 2007). The turbulent intensity was less than that encountered by Loehre for a similar solidity, but showed decay

similar to that of Roach. This reduced intensity can be attributed to smaller diameter holes and a difference in pressure drop across the screen. The variance in the mixing region was in agreement with that obtained from the work done by Mohamed.

This initial characterization of the single solidity perforated plates provided a baseline data set for comparison to plates of mixed solidities on the behavior of jet velocity decay. The characterization of the mixed solidity plates provided some useful information in the understanding of the interaction of perforated plate sections of different porosities. The free stream velocity predicted using the single solidity plate velocity decay calculations provided a prediction within the range of uncertainty. The plane mixing layer width for the mixed solidity plates where within the limits of the two combined solidity perforated plate sections. This is important in that each interaction between sections can be treated independently without accounting for other sections. The velocity ratio tested was also with the range of that tested that had a problem matching a velocity gradient. The mixed solidity tests did not show the same problem and leads to the conclusion that the contributing factor to the error associated with the velocity profile generating screens was from the solidities implemented that were close to the range where instabilities were associated. This will have to be verified in future tests, but it does provide a range in which a porosity-velocity relationship is identified to hold true. The final conclusion that can be made is that the mixing of perforated plates of different porosities can be shown to show the characteristics of self-preserving flow such as plane mixing layers. This observation provides a relationship that can be used to better predict the velocity between the sections of different porosities and an improvement of the velocity profile generating screen.

REFERENCES

Baines, W. (1951). An Investigation of FLow Through Screens. *Transactions of the ASME*, 467-480.

Elder, J. (1959). Steady Flow Through Non-Uniform Gauzes of Arbitrary Shape. *Journal of Fluid Mechanics*, 355-368.

Golsen, M. (2011). EXPERIMENTAL AND NUMERICAL INVESTIGATION OF AERODYNAMIC UNSTEADINESS IN A GAS TURBINE MIDFRAME. *University of Central Florida Thesis*.

Horender, S. (2013). Turbulent Flow Downstream of a Large Solidity Perforated Plate: Near-Field Characteristics of Interacting Jets. *Fluid Dynamics Research*.

Jorgensen, F. (2002). *How to Meaure Turbulence with Hot-Wire Anemometers.* Skovlunde, Denmark: Dantec Dynamics.

Laws, E. (1978). Flow Through Screens. *Annual Review of Fluid Mechanics*, 247-266.

Liu, R. (2004). On the Generation of Turbulence with a Perforated Plate. *Experimental Thermal and Fluid Science*, 307-316.

Liu, R. (2007). Constant Reynolds Number Turbulence Downstream of an Orificed Perforated Plate. *Experimental Thermal and Fluid Science*, 897-908.

Livesey, J. (1973). Simulation of Velocity Profiles by Shaped Gauze Screens. *AIAA Journal*, 184-188.

McCarthy, J. (1964). Steady Flow Past Non-Uniform Wire Grids. *Journal of Lfuid Mechanics*, 491-512.

Mehta, R. (1991). Effect of Velocity Ratio on Plane Mixing Layer Development: Influence of the Splitter Plate Wake. *Experiments in Fluids*, 194-204.

Mohamed, M., & Larue, J. (1990). The Decay Power Law in Grid-Generated Turbulence. *Journal of Fluid Mechanics*, 195-214.

Owen, P., & Zienkiewicz, H. (1957). The Production of Uniform Shear Flow in a Wind Tunnel. *Journal of Fluid Mechanics*, 521-531.

Papadopoulos, G. (1999). A Gerneric Centerline Velocity Decay Curve for Initially Turbulent Axisymmetric Jets. *Transactions of the ASME*, 80-85.

Roach, P. (1987). The Generation of Nearly Isotropic Turbulence by Means of Grids. *International Journal of Heat and Fluid Flow*, 82-92.

Schlichting, H. (1979). *Boundary-Layer Theory 7th Edition.* New York: McGraw-Hill Higher Education.

Smith, L. (1970). Casing Boundary Layers in Multistage Axial-Flow Compressors . *Flow Research on Blading*, 635-647.

Stearns, R. (1951). *Flow Measurements with Orifice Meters.* New York: Van Nostrand.

Svensson, K. (2015). Experimental and Numerical Investigation of Confluent Round Jets. *Linköping Studies in Science and Technology Dissertation No. 1653*. Linköping University.

Tan-Atichat, J. (1982). Interactino of Free-Stream Turbulence with Screens and Grids: A Balance Between Turbulence Scales. *Journal of Fluid Mechanics*, 501-528.

Tavoularis, S. (1987). The Structure of a Turbulent Shear Layer Embedded in Turbulence. *Phys. Fluids Vol 30*.

Townsend, A. (1976). *The Structure of Turbulent Shear Flow.* Cambridge: Cambridge University Press.

Turner, J. (1969). A Computational Method for the Flow Through Non-Uniform Gauzes: The General Two-Dimensional Case. *Journal of Fluid Mechanics*, 367-383.

Winkle, M., & Kolodizie, P. (1957). Discharge Coefficients through Perforated Plates. *AIChE Journal*, 305-312.